



Restructuring in block copolymer thin films: In situ GISAXS investigations during solvent vapor annealing



Dorthe Posselt^{a,*}, Jianqi Zhang^{b,c}, Detlef-M. Smilgies^{d,*}, Anatoly V. Berezkin^b, Igor I. Potemkin^e, Christine M. Papadakis^{b,*}

^a IMFUFA, Department of Science and Environment, Roskilde University, P.O. Box 260, 4000 Roskilde, Denmark

^b Technische Universität München, Physik-Department, Physik weicher Materie, James-Franck-Str. 1, 85748 Garching, Germany

^c National Center for Nanoscience and Technology (NCNST), No. 11 ZhongGuanCun BeiYiTiao, 100190 Beijing, PR China

^d Cornell High Energy Synchrotron Source (CHESS), Wilson Laboratory, Cornell University, Ithaca, NY 14853, USA

^e Physics Department, Lomonosov Moscow State University, Moscow 119991, Russian Federation

ARTICLE INFO

Article history:

Available online 23 September 2016

Keywords:

Solvent vapor annealing
Block copolymers
Thin films
Theory
Simulations
GISAXS

ABSTRACT

Block copolymer (BCP) thin films have been proposed for a number of nanotechnology applications, such as nanolithography and as nanotemplates, nanoporous membranes and sensors. Solvent vapor annealing (SVA) has emerged as a powerful technique for manipulating and controlling the structure of BCP thin films, e.g., by healing defects, by altering the orientation of the microdomains and by changing the morphology. Due to high time resolution and compatibility with SVA environments, grazing-incidence small-angle X-ray scattering (GISAXS) is an indispensable technique for studying the SVA process, providing information of the BCP thin film structure both laterally and along the film normal. Especially, state-of-the-art combined GISAXS/SVA setups at synchrotron sources have facilitated in situ and real-time studies of the SVA process with a time resolution of a few seconds, giving important insight into the pathways and mechanisms of SVA induced restructuring. We give a short introduction to the GISAXS method and review recent theoretical studies, experimental techniques such as sample preparation and in situ chambers together with SVA protocols, and we review and discuss experimental results. We conclude by giving an outlook on emerging developments of the in situ real-time GISAXS scattering technique in combination with new approaches to control BCP thin film structures using SVA.

© 2017 Elsevier B.V. All rights reserved.

Contents

| | |
|--|----|
| 1. Introduction | 81 |
| 2. Theoretical results and predictions | 83 |
| 2.1. Equilibrium structure of DBCP films in a slit | 83 |
| 2.2. Free-surface films | 83 |
| 2.3. Effect of solvent on the structure of BCP films | 85 |
| 3. Experimental developments | 88 |
| 3.1. Film preparation | 88 |

* Corresponding authors.

E-mail addresses: dorthe@ruc.dk (D. Posselt), dms79@cornell.edu (D.-M. Smilgies), papadakis@tum.de (C.M. Papadakis).

| | | |
|--------|---|-----|
| 3.2. | In situ sample environments for SVA..... | 89 |
| 3.2.1. | Chambers based on a reservoir containing liquid solvent..... | 89 |
| 3.2.2. | Chambers based on a flow of solvent vapor..... | 89 |
| 3.3. | GISAXS experiments | 92 |
| 3.4. | Interpretation of 2D GISAXS maps for lamellar systems..... | 93 |
| 4. | Results from experiments | 95 |
| 4.1. | Studies aiming at improving the lateral order | 95 |
| 4.2. | Studies aiming at controlling the orientation of the morphology | 96 |
| 4.3. | Studies aiming at altering the morphology..... | 98 |
| 4.4. | Real-time in situ studies of restructuring processes during SVA..... | 101 |
| 5. | Future application areas for in situ studies | 106 |
| 5.1. | Enhancement of scattering contrast | 106 |
| 5.2. | New approaches to SVA | 107 |
| 5.3. | Macroscopic orientation by combining SVA with other methods | 108 |
| 6. | Conclusion..... | 109 |
| | Acknowledgements..... | 110 |
| | References..... | 110 |

Nomenclature

| | |
|----------------------------------|--|
| AFM | atomic force microscopy |
| BCC | body-centered cubic |
| BCP | block copolymer |
| BR | Bragg rod |
| CCD | charge-coupled device |
| CHX | cyclohexane |
| DBCP | diblock copolymer |
| DBS | diffuse Bragg sheet |
| DDFT | dynamic density functional theory |
| DFT | density functional theory |
| DPD | dissipative particle dynamics |
| DSA | directed self-assembly |
| DWBA | distorted-wave Born approximation |
| EAC | ethylacetate |
| GISANS | grazing-incidence small-angle neutron scattering |
| GISAXS | grazing-incidence small-angle X-ray scattering |
| GIUSAXS | grazing-incidence ultra-small angle X-ray scattering |
| GIWAXS | grazing-incidence wide-angle X-ray scattering |
| HPL | hexagonally perforated lamellae |
| MC | Monte Carlo |
| MD | molecular dynamics |
| MEK | methyl ethyl ketone |
| ODT | order-to-disorder transition |
| OFTM | optical film thickness monitor |
| P2VP- <i>b</i> -PDMS | poly(2-vinylpyridine)- <i>b</i> -poly(dimethylsiloxane) |
| P α MS- <i>b</i> -PHOST | poly(α -methylstyrene)- <i>b</i> -poly(4-hydroxystyrene) |
| PHEMA- <i>b</i> -PMMA | poly(2-hydroxyethyl methacrylate)- <i>b</i> -poly(methyl methacrylate) |
| PI- <i>b</i> -PLA | polyisoprene- <i>b</i> -poly(D,L-lactide) |
| PI- <i>b</i> -PS- <i>b</i> -P2VP | poly(1,4-isoprene)- <i>b</i> -polystyrene- <i>b</i> -poly-(2-vinyl pyridine) |

| | |
|-------------------------------------|--|
| PS- <i>b</i> -P2VP | polystyrene- <i>b</i> -poly(2-vinylpyridine) |
| PS- <i>b</i> -P2VP- <i>b</i> -PtBMA | polystyrene- <i>b</i> -poly(2-vinylpyridine)- <i>b</i> -poly(<i>tert</i> -butyl methacrylate) |
| PS- <i>b</i> -P4VP | polystyrene- <i>b</i> -poly(4-vinylpyridine) |
| PS- <i>b</i> -PB | polystyrene- <i>b</i> -polybutadiene |
| PS- <i>b</i> -PB- <i>b</i> -PS | polystyrene- <i>b</i> -polybutadiene- <i>b</i> -polystyrene |
| PS- <i>b</i> -PDMS | polystyrene- <i>b</i> -poly(dimethylsiloxane) |
| PS- <i>b</i> -PEO | polystyrene- <i>b</i> -poly(ethylene oxide) |
| PS- <i>b</i> -PNIPAM- <i>b</i> -PS | polystyrene- <i>b</i> -poly(N-isopropyl acrylamide)- <i>b</i> -polystyrene |
| SAXS | small-angle X-ray scattering |
| SCFT | self-consistent field theory |
| SEM | scanning electron microscopy |
| SSL | strong segregation limit |
| SVA | solvent vapor annealing |
| THF | tetrahydrofuran |
| WSL | weak segregation limit |

1. Introduction

Nanostructured polymer thin films can be prepared by a wealth of methods [1,2]. Among these, BCP thin films have proven to be of special interest for a number of nanotechnology applications, such as nanolithography [3–11] and sensors [12–14], as templates for the fabrication of functional arrays [15–25], and for the fabrication of nanoporous films and membranes [23,26–32]. BCP thin films self-assemble on the mesoscale with a characteristic length scale of ~10–100 nm and film thicknesses of ~1–20 times this value.

For most applications, it is necessary to control different aspects of the BCP thin film structures, such as the specific mesostructured morphology, the length scale and the orientation of mesostructures as well as the degree of order. Moreover, a replacement of selected microdomains by functional materials requires careful consideration when tailoring the two parts of the BCP, and further processing

requires robustness of the structures. The physics and applications of BCPs in the bulk and in thin film geometry have been reviewed previously [32–37].

A versatile procedure for preparing BCP thin films of well-defined thickness is spin coating. By controlling the spin coating parameters, films of different thickness can be obtained. Partially because of the fast evaporation of the solvent, spin coated BCP thin films are typically not in thermal equilibrium. They often show kinetically trapped and defect-rich morphologies, which necessitates the application of an annealing method. Among other methods, SVA has emerged as a powerful technique with a potential for fine tuning the BCP thin film morphology. In SVA, a BCP thin film is exposed to the vapor of a solvent and is swelled to a certain controlled degree before being dried at a rate which often also is under control. As a result, defects are removed, the correlation length of the microdomain order is increased and, in certain cases, the morphology orientation or type is changed. By varying solvent quality and selectivity toward the different BCP blocks, the maximum degree of swelling and the drying rate, it is possible to obtain a high degree of control over the annealing process. Pioneering work was carried out by Krausch and coworkers [38,39] who also designed cells for first *in situ* measurements during SVA.

A number of new developments make the SVA process interesting for semiconductor processing, such as the development of very fast treatment protocols [40]. The combination of SVA with other protocols, such as DSA [41–43], allows preparation of ordered morphologies over macroscopic dimensions, which brings BCP thin films closer to applications, e.g., in nanolithography. The latest frontier in this approach has been to develop methods getting below the 20 nm limit of the most advanced lithography techniques by applying top down methods to orient self-organized BCP with feature sizes down to 5 nm [44]. A recent review summarizes the development and state of the art [45].

The detailed restructuring mechanisms taking place during SVA still contain many unexplored aspects, and observing and understanding these mechanisms will expand the ability to tailor mesostructured BCP thin films to specific needs. Due to the huge parameter space, it is, *a priori*, not straightforward to choose the appropriate conditions when using SVA to induce a certain structure in BCP thin films: The choice of the BCP implies a certain equilibrium morphology and repeat distance, which, for an AB DBCP, are determined by the composition, i.e. the volume fraction of one of the blocks, e.g., the A block, f_A , the overall degree of polymerization, N , and the Flory–Huggins segment-segment interaction parameter between the two blocks, χ_{AB} , which is related to the interfacial tension between the microdomains. Moreover, the film thickness, h , the chemical and topological properties of the substrate and its resulting interactions with the blocks of the BCP, as well as the surface tensions of the two microdomains, γ_A and γ_B , are of importance. The content of annealing solvent in the film, its quality and selectivity, i.e. the difference in the solvent quality between the blocks, may have an effect on the pathway and kinetics of the structural changes as well as the resulting structure. Moreover,

the maximum degree of swelling influences, whether the BCP thin film (i) becomes disordered in the swollen state and eventually may order again during drying or (ii) the film stays in the ordered state where structural changes become possible because of increased polymer mobility during solvent uptake, e.g., because glassy microdomains become viscoelastic. Finally, the rates of swelling and drying may play a role, and fast drying may result in kinetically trapped or metastable states. It is thus highly desirable to identify general rules for navigating the complex parameter space.

A recent review has summarized significant results obtained by SVA until 2012 [46] giving details about the choice of polymer system, substrate, polymer deposition processes and solvent conditions. It was pointed out that GISAXS is the key method for structural investigations of dry and swollen polymers, however, the review does not feature any details about the GISAXS method and the interpretation of GISAXS maps. Since then, there has been a rapid increase in studies using sophisticated SVA protocols and equipment to elucidate pathways of structural changes, and it is the aim of the present review to focus on current knowledge of restructuring mechanisms as obtained by GISAXS, and link this, when possible, to theoretical advances. A review published after submission of the present review [47] gives an overview of possible uses of different *in situ* X-ray and neutron scattering techniques for investigation of different ways to anneal block copolymer thin films. Finally, a recent review has addressed fast ordering techniques for block copolymer films including a brief section on SVA [48].

The purpose of the present review is to summarize *in situ* investigations using GISAXS during SVA, both when the film is in equilibrium at a certain degree of swelling, and when the film is restructuring during SVA, i.e. in non-equilibrium. The latter case requires *time-resolved* GISAXS measurements. A number of theoretical studies have addressed the mechanisms of structural reorganization during SVA, these are reviewed in Section 2. Section 3 describes the main methodology of film preparation and SVA, focusing on the development of chambers designed for SVA. We describe the main method currently used to investigate the structural changes, namely *in situ* GISAXS. The fundamentals of the GISAXS method have been reviewed previously [49–55]; and we will therefore only provide a brief introduction together with a short description of the data analysis strategies. Section 4 is devoted to review the results described in the literature and is divided into four subsections describing studies aiming at (i) improving the degree of lateral order, (ii) controlling/altering the orientation of the morphology, (iii) altering the morphology and (iv) understanding the mechanisms of structural reorganization. Many of these investigations are *in situ* equilibrium studies, i.e. GISAXS data are taken in the as-prepared state, at certain degrees of swelling and after drying. *In situ* real-time GISAXS studies have become increasingly popular, and we show that these studies provide a wealth of information on the pathways and the relevant time scales for restructuring. Finally, in Section 5, the review points out challenges and future directions of the field.

2. Theoretical results and predictions

This section summarizes current understanding of physical aspects guiding nanostructure formation and relaxation in BCP thin films during SVA. In practice, SVA most often starts with a non-equilibrium BCP thin film and is aimed at equilibration of the nanostructure after solvent evaporation. Therefore, the most important issues in the theoretical considerations of SVA are (i) the equilibrium structure of the pure BCP thin films without solvent and (ii) the evolution of the structure during the different stages of SVA. Equilibrium structures of thin BCP films have been studied theoretically and with computer simulations in great detail, as discussed in Sections 2.1 and 2.2. However, the question of structural evolution during solvent uptake and its further evaporation, discussed in Section 2.3, is still open and has only been considered in few recent publications. Progress in answering this question is important for fine-tuning the SVA process and is expected to stimulate further experimental studies.

2.1. Equilibrium structure of DBCP films in a slit

The thermodynamic incompatibility between the A and B blocks drives the self-assembly of similar blocks into microdomains, having shapes and distributions which are balanced to minimize unfavorable A/B contacts and maximize the conformational and translation entropy of the DBCP. In the bulk, the microphase separation of DBCPs results in different well-known ordered morphologies. With the volume fraction f_A increasing from 0 to 0.5, the body-centered cubic morphology with A spheres in a B matrix, hexagonally packed A cylinders in a B matrix, the bicontinuous gyroid phase, and the lamellar morphology are encountered in the given order [33,36]. In thin films, confinement decreases the entropy of BCP films, simultaneously increasing the diversity of possible microdomain morphologies. As mentioned above, the film thickness, h , and polymer–surface interactions are additional parameters compared to bulk, controlling the conditions for microphase separation and the resulting morphology.

As the simplest case, most theoretical studies have dealt with the films confined between two solid walls in order to introduce the confinement symmetrically and to reduce the number of independent variables. The pioneering theoretical investigations [56–61] focused on self-assembly of symmetric, lamellae-forming DBCPs, and only during the last decade, the effect of copolymer compositions (f_A) different from 0.5, i.e. asymmetric DBCPs, was intensively studied [62–79]. Most of the confined copolymer films have been investigated in the weak segregation regime using SCFT [70,72,73,75,79,80] and DDFT [62,63,65,67,76,77]. The strong segregation regime was considered in computer simulations with the bond fluctuation model [66,78] as well as using thermodynamic scaling theories [68,69,74]. The corresponding phase diagrams can be found in Refs. [62–67,70–73,76–79], and a recent paper by Li et al. [79] presents a comprehensive review of the field.

Even in the simple case of identical walls, the morphologies of confined BCP films are exceptionally diverse, as seen in Fig. 1 [79]. The film structure is primarily

controlled by the (in)commensurability of the film thickness (h) and the characteristic size of the mesostructure, one measure of which is the radius of gyration of the BCP (R_g), and by f_A . An incommensurability can be resolved by a vertical microdomain orientation, especially in thin films and for symmetric copolymers forming the lamellar morphology [59–61], by alternative microdomain ordering [73], by a change of the size of the microdomains and of the repeat distances [78] or by undulations of microdomains [70,78] within the films. Undulating lamellae and cylinders, and lying cylinders with non-integer period have also been predicted as possible structures in confinement [70]. The thermodynamic stability of some of these morphologies is still subject to discussion [75,79]. The following thin film morphologies seen in Fig. 1a have been investigated experimentally (Section 4): parallel (e.g., L_1^{\parallel} , L_2^{\parallel} – the short notation refers to Fig. 1) and perpendicular lamellae (L_{\perp}), standing (SC) and lying cylinders (e.g., C_1 , C_2), and spheres (e.g., S_1 , S_2). In the following, we will refer to perpendicular lamellae and standing cylinders as “vertical morphologies”. Moreover, ultrathin and thin films are distinguished: In ultrathin films, the film thickness is of the order of the repeat distance (upper row of Fig. 1a), whereas in thin films, it is larger (lower rows of Fig. 1a), but not so large that the confinement effect becomes negligible.

A number of theoretical studies were aimed at understanding the effect of selective block adsorption [59,63–65,69,71,72,74,81–83] which is often relevant in experiments. Selective wetting as well as commensurability between the film thickness and the microdomain size of the DBCP stabilize the parallel lamellar orientation of symmetric DBCPs [59,83]. In contrast, films from asymmetric DBCPs under the same conditions form various *mixed morphologies* [63,68,71,72,79,84], where the morphology and the microdomain orientation are different near the film interfaces and in the core of the film.

2.2. Free-surface films

Most of the BCP thin films studied experimentally are prepared on a solid substrate and have a free polymer–air interface. In such films, incommensurability between characteristic dimensions of the microdomain morphology and the film thickness can be relaxed via both the domain reorientation or by the formation of “terraced” structures, islands, or holes [33,38,65,67,81,84–86], resulting in an inhomogeneous film thickness. The latter mechanism is energetically preferred if one or both of the interfaces possess an affinity to one of the copolymer blocks, which facilitates the horizontal orientation of domains. An odd number of layers in the terraced film will be stable when both interfaces have an affinity to the same block, while in the opposite case, even numbers of layers appear. Films with a free surface were considered in few theoretical studies of symmetric [69,74,87–89] and asymmetric [38,65,67] DBCPs. These studies demonstrated that symmetric DBCPs have a lamellar morphology also in confinement, while the number and orientation of the lamellae are controlled by the Flory–Huggins interaction parameter, χ_{AB} , the equilibrium film thickness, and also by the polymer–substrate and polymer–air interactions, which can be expressed through

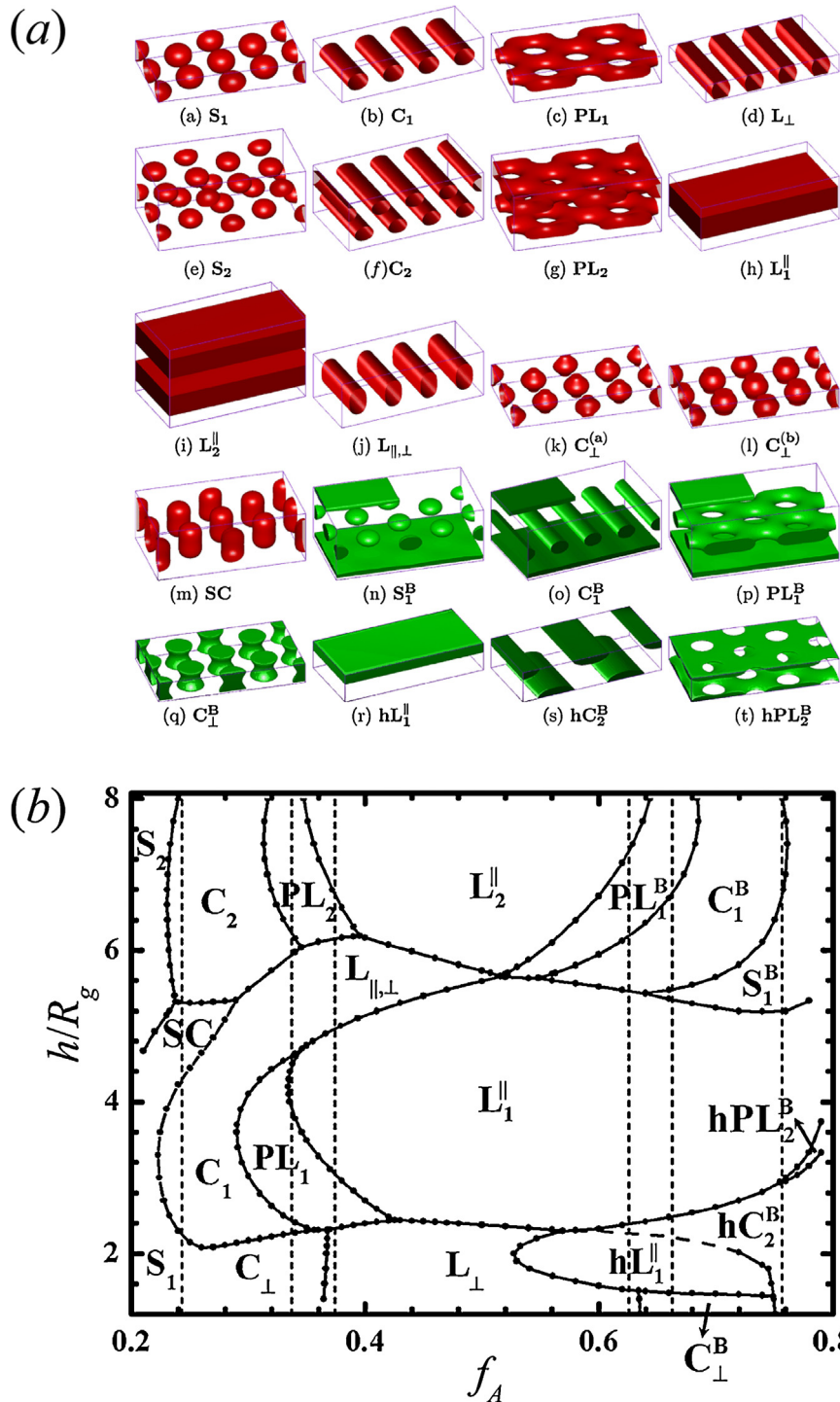


Fig. 1. Theoretical DBCP thin film morphologies confined between two selective walls (a) and corresponding phase diagram (b). The walls preferentially adsorbing the major or the minor blocks are indicated in red and green, respectively. The phase diagram was calculated at $\chi_{ABN} = 20$ (χ_{AB} is the Flory–Huggins segment–segment interaction parameter and N the degree of polymerization of the DBCP) in dependence on the volume fraction of the A block, f_A , and the ratio of film thickness, h , to the radius of gyration of the DBCP, R_g [79]. Copyright 2013. (For interpretation of the references to colour in this figure legend, the reader is referred to the web version of this article.)

Source: Reproduced with permission from the American Chemical Society.

the spreading parameters, S_A and S_B [87]. The spreading parameters depend on the surface tension coefficients, γ_{ij} , as $S_A = \gamma_{sa} - (\gamma_{As} + \gamma_{Aa})$ and $S_B = \gamma_{sa} - (\gamma_{Bs} + \gamma_{Ba})$ where the subscripts A, B, s and a indicate the two different blocks (A and B) and the substrate and air (s and a), respectively. For a vertical orientation of the lamellar microdomains in symmetric DBCPs, the spreading parameters have to be similar. Extension of this theory into the intermediate segregation regime [88] demonstrates that high molar mass stabilizes the perpendicular lamellar orientation, whereas low molar mass DBCPs form parallel lamellae. In thin films from asymmetric copolymers [38,65,67], diverse mixed morphologies may appear due to reconstruction in the vicinity of the free film interface.

2.3. Effect of solvent on the structure of BCP films

Theoretical approaches to describe the role of the solvent in BCP thin films during SVA has only recently been attempted. A number of different approaches was used to understand the effect of a solvent in equilibrium [90–95] and at different stages of SVA [94,96–103] on the structure and microdomain orientation in BCP thin films, using MD simulations [96,98,100–102], MC simulations [90,91,95], the Flory–Huggins Cahn–Hilliard model [97], SCFT [80,92], DFT [93,103], DPD [94,102,104], and analytical theory [99,105]. Most of these studies consider the case of fast solvent evaporation resulting in a large gradient of the solvent concentration in the BCP film. Also, these models are incomplete because they do not take into account the experimentally important case that microdomains may change from the glassy to the viscoelastic state upon SVA, which drastically alters the molecular mobility and the relaxation rate – such theories assume the viscoelastic state throughout. Thus, the structural changes obtained in these simulations are mostly due to, for instance, a spatially non-uniform altering of the interfacial tension between the different blocks by a non-selective solvent distributed inhomogeneously throughout the film, or by the change of the morphology due to selective solvent absorption in the different BCP microdomains. A recent experimental example of this effect is given in Ref. [106]. In the following, we discuss the solvent screening effect, non-equilibrium effects, the stability of different microdomain orientations against film swelling and drying, and the role of the strength of block segregation and of solvent selectivity.

Screening effect. A non-selective solvent being added to a BCP diminishes unfavorable contacts between immiscible components. In the so-called dilution approximation by Helfand and Tagami [107], this screening leads to the scaling of the repeat distances of ordered microdomain structures with the volume fraction of the polymer ϕ_p , in a polymer–solvent mixture due to the change of the effective interaction parameter, $\chi_{\text{eff}} = \phi_p \chi_{AB}$. Using SCFT, it has been shown [107–109] that the ODT in swollen films occurs at $\chi_{\text{eff}} N \approx 10.5$ for both non-selective and selective solvents, i.e. analogous to the ODT condition in non-swollen films. In the ordered state, solvent uptake causes growth of the interdomain surface area, and *domain thinning* which approximately follows the scaling law $D_{\text{lam}} \propto$

$\chi_{AB}^p N^q \phi_p^\beta$, identified both theoretically [94,108–111] and experimentally [110,112–118]. For symmetric copolymers in non-selective solvent, the lamellar thickness is predicted to scale in the WSL with $p \approx 1/3$, $q \approx 0.8$, and $\beta \approx 0.4$, and in the SSL with $p \approx 0.2$, $q \approx 2/3$, and $\beta \approx 0.2$ [108]. Taking into account the finite width of the lamellar interfaces, i.e. going beyond the SSL, results in $p = 1/6$, $q \approx 2/3$, and $\beta = 1/6$ for lamellae in non-selective solvent [111]. The effect of highly selective solvents is more complicated, because swelling may affect the morphology [119]. At $\chi_{SA} = 0$ and $\chi_{SB} = \chi_{AB}$ (where S, A , and B denote the solvent and the A - and B -blocks), SCFT calculations [109] give $p \approx 0.5$, $q \approx 0.9$, $\beta \approx 0.5$ in the WSL, and $p \approx 0.2$, $q \approx 0.7$, $\beta \approx 0.2$ in the SSL. In experimental studies [115–117] focusing on selective solvents, β has been shown to vary from 0.51 to –0.46, but for systems well above the glass transition, experiments [109,112–115,117,118] have identified β -values relatively close to the theoretical value of 1/3, while below the glass transition and at smaller solvent concentrations ϕ_S ($\phi_S < 0.3$), even negative values, e.g., $\beta = -1$, were observed [112], which was explained by non-equilibrium one-dimensional swelling. It is an important question whether this increase or decrease of the repeat distances observed in the bulk is present in thin film geometry where confinement effects and the difficulty of large-scale mass transport may play a role [111,120,121].

Non-equilibrium effects in SVA. Experiments have demonstrated that the final film morphology is affected by the conditions of SVA and may notably deviate from the equilibrium one. Thus, SVA can create non-equilibrium but practically interesting structures, such as vertically oriented domains on selective substrates, or diverse morphologies from the same copolymer [80,106]. Despite significant theoretical progress, such effects of SVA are not well understood yet. Most researchers agree that the formation of non-equilibrium morphologies is driven by intense solvent flows through the polymer film upon swelling, and especially during drying.

A first simulation of the effect of solvent evaporation on a film from symmetric DBCPs was done in 2004 by Tsige et al. [96] using MD simulations. Considering the case of a non-selective surface and a non-selective solvent, they could show that a gradient of the solvent concentration within the film tend to orient the microdomains vertically, i.e. with their long axis along the substrate normal; however, this effect was quite weak. Later, Buxton and Clarke [97] using the Cahn–Hilliard theory and Morita et al. [98] using DPD simulations reproduced the orienting effect of a gradient of a non-selective solvent even in films of two immiscible homopolymers. These results demonstrated that the binding of polymers into BCPs may play a secondary role in the domain reorientation. At present, different mechanisms and prerequisites of the solvent gradient orienting effect have been discussed in the literature. It is quite possible that, depending on the nature of the copolymer, the solvent and the SVA protocol, different combinations of the phenomena are responsible for the thin film reconstruction. Among important factors under discussion are the morphological transformations of microdomain structures upon drying, the strength of the dry block segregation, the solvent selectivity

and the relative rate of solvent diffusion in the different blocks, polymer self-assembly and defect relaxation in the microdomain structure, and interfacial phenomena such as non-trivial solvent and polymer transport on the interfaces between domains, including the Gibbs-Marangoni effect [100].

Stability of different microdomain orientations against film swelling/drying. The recent DPD simulations by Rudov et al. [94] demonstrated that parallel and perpendicular lamellae have different stability against swelling in a non-selective solvent. The initial orientation was controlled by the selectivity of the substrate toward the two blocks, in full agreement with the theory given in Ref. [87]. Swelling reduced the effective repulsion between blocks and caused thinning of domains, as predicted by Helfand and Tagami [107]. However, this thinning requires a complete reconstruction of parallel lamellae, while perpendicular lamellae “survive”, simply being stretched and tilted, as seen in Fig. 2 [94]. This different stability of differently oriented domains upon one-dimensional film swelling or drying can be one of the main mechanisms of domain reorientation.

The strength of the dry block segregation was found to be important to produce ordered morphologies by SVA [95,99,103,104]. In all these simulations, ordered defect-free perpendicular lamellae appeared within a certain range of block segregations above the ODT, i.e. in the WSL. A further increase of block segregation suppresses the relaxation of defects, thereby preventing the formation of defect-free morphologies [95,104], because a higher interfacial tension creates a larger free energy barrier for the relaxation of defects.

Hur et al. [95] analyzed the effect of the block segregation above the ODT, i.e. in the WSL, using also a coarse-grained MC simulation of swelling and subsequent drying of a thin film of symmetric DBCPs in a non-selective solvent. The authors introduced the activation energy of microdomain relaxation, related to the effective degree of segregation, which is proportional to $\chi_{eff}N$. Then, the average time of defect annihilation, τ , scales as $\tau \propto \zeta^2 \exp(a\chi_{eff}N)/D_0$, where ζ is the size of the defect, D_0 the diffusion coefficient of the DBCP, and a is a constant. In Refs. [95,119], the defect annihilation time was found to be comparable for different initial solvent concentrations in the film. From this result, the authors concluded that DBCPs with large $\chi_{eff}N$ values in the swollen state are less likely to form defect-free structures.

Solvent selectivity is especially important for SVA of thin films from asymmetric BCPs. Such films from cylinder forming copolymers were considered theoretically by Phillip et al. [99], Paradiso et al. [103] and by Berezhkin et al. [104]. In Ref. [104], the effect of solvent selectivity and quality on the cylinder orientation was systematically studied over a wide range. It was shown [103,104] that a certain solvent selectivity toward the majority blocks is necessary for a vertical domain orientation to compensate for the known preferential entropy-driven adsorption of the minority blocks at neutral interfaces [62,64,67]. Non-selective solvents in SVA of asymmetric BCPs led eventually to disordering, while selectivity toward the short block stabilized parallel cylinders [104]. In none of these cases, the film thickness affected the domain orientation.

Different mechanisms were proposed for the final appearance of vertical cylinder orientation. Phillip et al. [99] using analytical theory and Paradiso et al. [103] explaining their DDFT results, stated that, at high solvent concentration, the film is disordered due to screening of block segregation by the solvent, while the ODT may take place at low solvent concentration. Since a gradient of solvent concentration forms in the film at high solvent evaporation rates, evaporation initiates locally an ODT in the interfacial region, whereas the core of the swollen film stays disordered. The ordered phase at the free film surface directs further microdomain formation and growth. In the work of Phillip et al. [99], the ordered phase was assumed to appear via nucleation of spherical domains, which then transform into standing cylindrical domains for the case of cylinder-forming DBCPs. The authors expected the rate of the cylinder growth to be determined by both, the polymer diffusion coefficient and by the thermodynamic driving force toward microphase separation. This layer drifts with time along the film normal through the disordered film from the free surface toward the substrate and leaves behind a well-ordered vertical morphology, as illustrated in Fig. 3.

A different mechanism of domain orientation was observed in recent DPD simulations [104]. DPD captures thermal fluctuations and a large difference in the characteristic rates of polymer and solvent diffusion. Upon evaporation of the solvent, being selective to the majority block, first, the formation of disordered microdomains took place, starting near the free surface of the film, and then propagated down to the substrate. As soon as micelles appeared, dispersed throughout the film, they merged into worm-like cylindrical microdomains, as illustrated in Fig. 4. The vertical orientation of the microdomains starts homogeneously everywhere in the film after evaporation of more than half of the solvent. This agrees with the fact, that the solvent diffusion and evaporation rate exceed the rate of polymer diffusion and relaxation by several orders of magnitude.

The vertical orientation of microdomains in Ref. [104] was explained by the diffusion-driven solvent movement through the system of microdomains, which have different viscosities and permeabilities in a selective solvent, as well as by the movement of components along interdomain interfaces, triggered by the gradient of interfacial tension, the so-called Gibbs-Marangoni effect [100]. In that case, the orientation of the microdomains within the film can have a pronounced effect on the solvent diffusion and morphological changes in films during SVA, especially when the solvent concentrates at the interfaces between the microdomains. It has been shown [94,102] that DBCP films with vertical microdomain orientation swell and relax notably faster than in the case of the parallel orientation for two reasons. The relaxation of vertical morphologies proceeds through simple reorientation of microdomains and altering of their size, while evolution of the parallel morphologies involves a time-consuming microdomain reconstruction and large-scale mass-transport. In addition, interdomain interfaces play the role of diffusion pathways in strongly segregated copolymer films [102], and this facilitates solvent transfer in vertical microdomain structures.

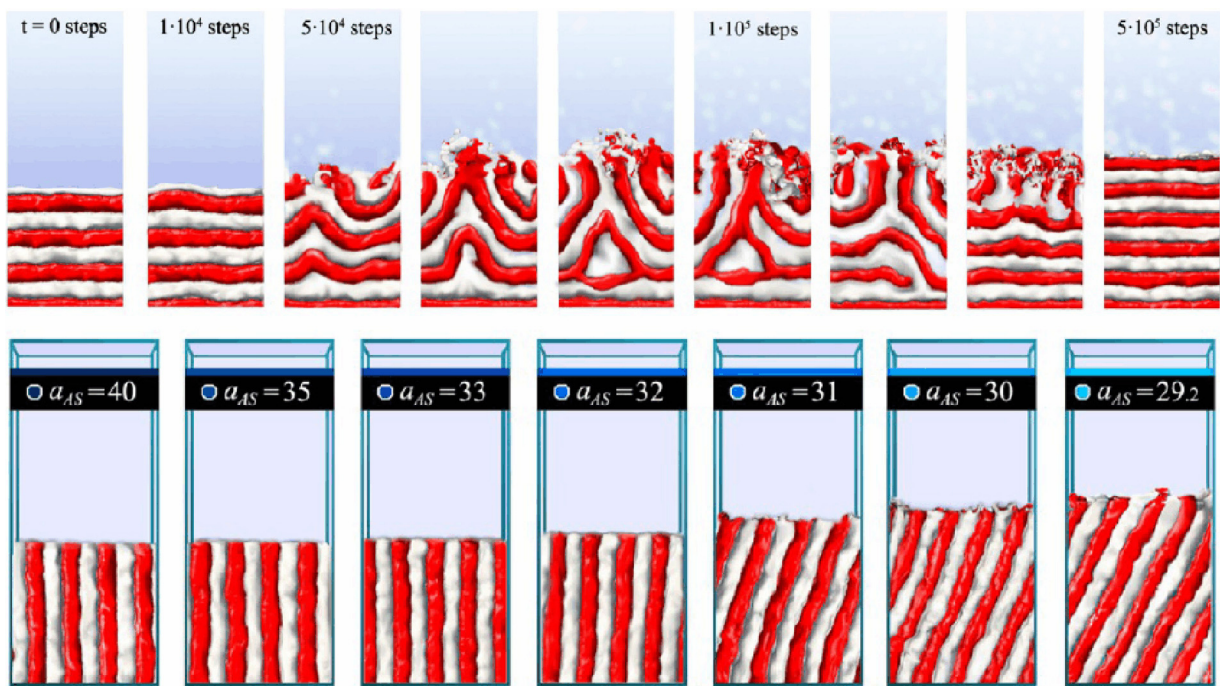


Fig. 2. Reconstruction of parallel (upper row) and perpendicular (bottom row) lamellae upon swelling in dependence on the degree of swelling (i.e. swelling time for parallel lamellae and the solvent quality for perpendicular lamellae). In the upper row, the repulsion parameter $a_{AS} = a_{BS}$ is proportional to the Flory–Huggins interaction parameter of the polymer–solvent interactions (non-selective solvent) [94]. Copyright 2013. Source: Reproduced with permission from the American Chemical Society.

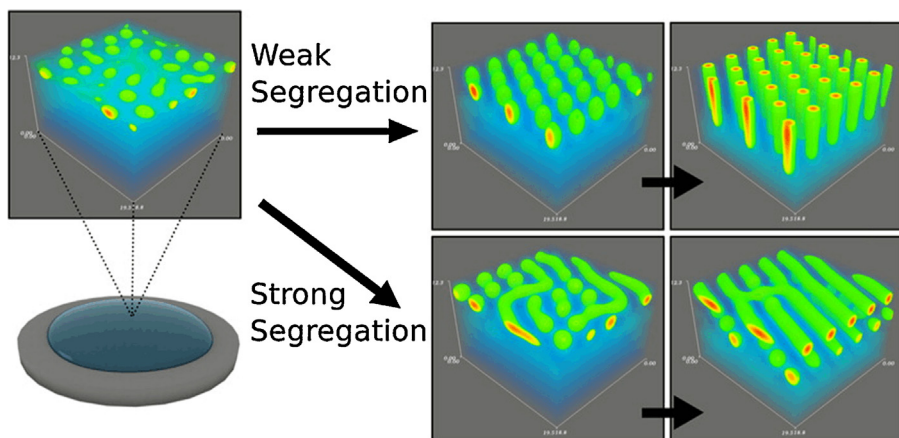


Fig. 3. Structure formation near the surface of a thin film from asymmetric DBCPs during drying from the fully swollen and disordered state (left). Depending on the initial segregation strength, standing (right, top row) or lying cylinders (right, bottom row) are formed during drying at a given evaporation rate. The color scale indicates the concentration of the two types of segments (blue: majority block, red: minority block). The solvent was non-selective [103]. Copyright 2014. (For interpretation of the references to colour in this figure legend, the reader is referred to the web version of this article.) Source: Reproduced with permission from the American Chemical Society.

Structures with more “direct” diffusion pathways also swell and dry faster in comparison with those having “entangled” interfaces. One can expect that fast and thus inhomogeneous drying of BCP thin films discussed above can lead to straightening of the diffusion pathways and, as a result, to microdomain transformation and orientation.

Summarizing this section, theoretical investigations have given a number of important insights into the possible mechanisms of SVA. It has been shown that BCPs, being

confined in thin films, demonstrate an enormous morphological diversity (more than 20 different morphologies in confinement between two solid walls). The morphology is controlled by block segregation strength, BCP composition, ratio between chain size and film thickness, and by BCP–surface interactions. Selectively adsorbing walls stabilize the parallel microdomain orientation, when there is commensurability between the repeat distance of the microdomain structure and the film thickness. Between

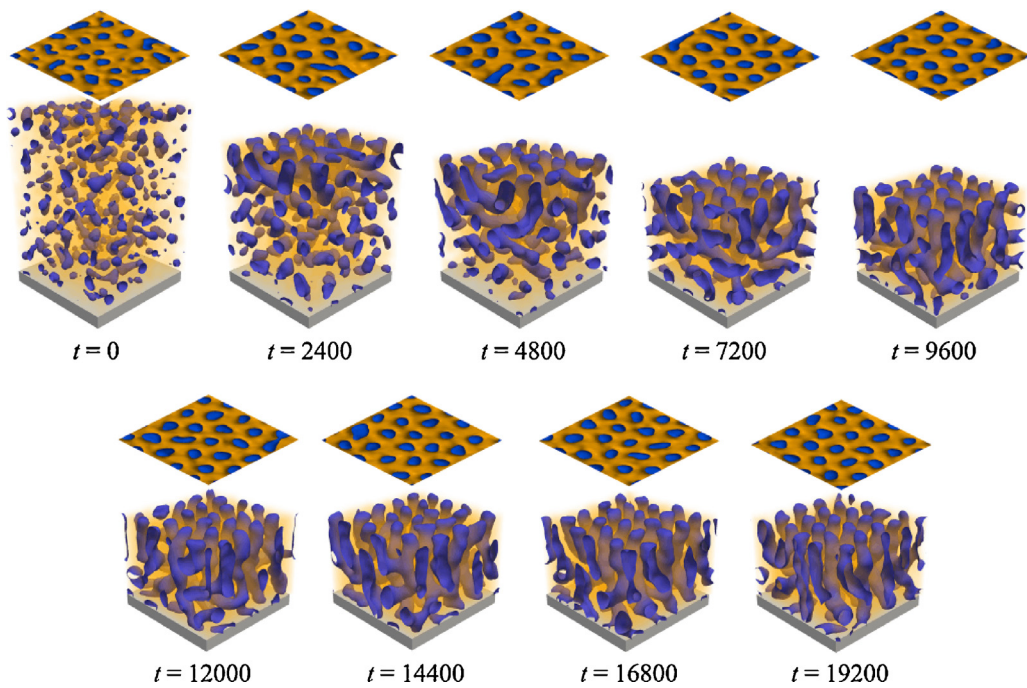


Fig. 4. Internal structure of the film and topography of the free surface at different stages of DPD simulation, starting from the swollen state in a solvent slightly selective toward the majority B blocks. Minor (A) and major (B) phases are shown in blue and yellow, respectively [104]. Copyright 2016. (For interpretation of the references to colour in this figure legend, the reader is referred to the web version of this article.) Reproduced with permission from the American Chemical Society.

non-selective surfaces and in case of incommensurability, parallel, vertical and mixed morphologies may appear, depending on the detailed conditions.

The equilibrium microdomain orientation and possibly the morphology itself can be adjusted by varying the solvent evaporation rate from the swollen film, the selectivity of the solvent and the block segregation. In addition, quenched nanostructures can be formed under high solvent evaporation rates, their microdomain orientation being also controlled by the selectivity of the solvent and the segregation strength of the BCP. For instance, the metastable vertical orientation of cylindrical microdomains in asymmetric DBCPs requires a weak or moderate solvent selectivity to the majority blocks, weak block segregation, and an ODT during the SVA [104]. Too strong block segregation suppresses the relaxation of defects in the microdomain structure.

Despite significant theoretical progress, many aspects of SVA remain unclear. Only a narrow range of block segregation strengths and polymer–solvent interactions has been studied up to now, and the roles of SVA kinetics, film thickness, solvent selectivity and possible memory effects are poorly understood yet. Further theoretical studies and computer simulations in the field are clearly needed.

3. Experimental developments

In this section, we describe typical protocols for film preparation together with designs of sample chambers, which have been developed for GISAXS experiments during SVA. Then, we present custom setups for *in situ* GISAXS

experiments and SVA protocols and give examples how GISAXS maps from representative BCP thin films are interpreted.

3.1. Film preparation

For GISAXS experiments, BCP thin films are most often prepared by spin coating from solution onto pre-cleaned Si wafers, because it is a fast and simple technique to prepare thin films of homogeneous thickness and high surface quality. The film thickness may be varied both by changing the polymer concentration in the solvent and by changing the spinning speed [122]. Typical spinning speeds range between 1000 and 3000 rpm and polymer concentrations between 5 and 30 mg/mL providing low-viscosity solutions. The choice of solvent – non-selective for all the different blocks or selective for one of them – may have an influence on the mesoscopic structures present in the spin coated film, and it is crucial for the wetting properties on the pre-cleaned substrates. After spin coating, the films are usually dried in vacuum, either at room temperature or at elevated temperature, to remove residual solvent from the film [123].

Silicon wafers have proven to be ideal substrates for GISAXS. Wafers are highly polished to low surface roughness and are extremely flat and chemically clean, matching the requirements of the semiconductor industry; wafers with a thin (a few nm) native oxide layer feature a low scattering background, and the amorphous thin oxide layer generates an isotropic surface on which materials are free to self-organize. In order to remove residual

contaminations and to provide reproducible casting conditions for the polymer films, the wafers are usually pre-cleaned in the lab. Among several, procedures are: (i) Piranha cleaning [124,125], which removes organic residues and certain metals, but may result in increased surface roughness, or milder protocols using other kinds of acidic aqueous solutions [121], (ii) dry wafer cleaning, e.g., snow jet cleaning using CO₂ [126], which removes micron and submicron particulates and hydrocarbon-based contamination, but may be tedious to use for large areas, and (iii) ultraviolet-ozone cleaning [111]. While these procedures result in hydrophobic surfaces, basic baths have been used for creating hydrophilic substrates for spin coating thin films of hydrophilic polymers dissolved in polar solvents [127].

The typical sample sizes for static GISAXS experiments can be relatively small – a length of 1 cm along the beam is sufficient for typical applications (for a discussion of the GISAXS scattering geometry see Section 3.3). For larger beam sizes, longer samples are needed to avoid overspill of the beam which not only causes loss of intensity but may also result in parasitic scattering from the support. For time-resolved GISAXS studies during SVA, radiation damage by the X-ray beam may occur for prolonged exposition and must be avoided. Therefore, after each measurement, the sample is moved such that a pristine spot is exposed to the beam during the investigation. Thus, the sample width may be chosen to be a few cm in order to ensure that a particular area is only exposed a limited amount of time, when the step width is chosen according to the beam width.

3.2. *In situ* sample environments for SVA

In this section, we describe recently developed sample environments for *in situ* GISAXS experiments during SVA. The development was triggered by the pioneering work of Krausch and coworkers using a chamber containing liquid solvent [38] and a chamber with a wet gas stream using a bubbler as well as temperature control of the sample [39]. These chambers enabled *in situ* imaging of thin BCP films by optical microscopy as well as monitoring the swelling of various homopolymer and BCP thin films during SVA using ellipsometry. For GISAXS, chambers containing liquid solvent in a reservoir have been frequently used [128–134]. Moreover, the vapor pressure in the chamber may be controlled by an additional flow of dry gas which facilitates stepwise swelling [111,135]. Such set-ups are advantageous for studies very close to saturation vapor pressure. The use of bubblers enables control of the film swelling, i.e. the swelling rate and the maximum degree of swelling, and of the drying process, i.e. the drying rate [121,136–140], particularly at vapor pressure maxima well below saturation. The most advanced set-ups use mass-flow controllers [141].

3.2.1. Chambers based on a reservoir containing liquid solvent

This mode is particularly effective, when solvent vapor close to the saturation level is needed [142]. In an early type of chamber for *in situ* GISAXS during SVA (Fig. 5a), liquid solvent was injected remotely into a reservoir below

the sample [120,143]. The chamber was closed and featured Kapton windows for the X-ray beam. Kapton is often chosen because of its chemical inertness to aggressive solvents such as acetone and its good stability in intense X-ray beams together with low absorbance. A small light bulb was used to heat the chamber and window slightly from the inside to avoid solvent condensation on the windows. This way, a close to saturated vapor atmosphere was installed in the chamber. Using this type of chamber, the film thickness typically increases rapidly after solvent is injected and levels off after some time, which, depending on the chamber size, is typically a few minutes (Fig. 5b).

To slow down the swelling process, an inert gas flow (typically helium or nitrogen) through the chamber can be employed and varied between 0 and typically a few hundred standard cubic centimeters per minute (Figs. 5c and 6, [120,144]). In this case, the flow is kept parallel to the sample surface and ~1 cm above the surface plane, thus facilitating turbulent mixing with the solvent vapor while avoiding direct interaction with the films. The higher the gas flow, the lower is the local organic vapor pressure at the sample. This way, the BCP thin film could be swollen to a certain extent, and this film thickness could then be kept constant sufficiently long time to achieve equilibrium (stepwise swelling, Fig. 5d, [111]).

In many studies, an OFTM (e.g., a white-light interferometer by Ocean Optics or a spectroscopic reflectometer by FilMetrics) has been used to measure the film thickness *in situ* during SVA [129,135,145]. The OFTM is coupled to a lens assembly and a CaF₂ window in the chamber via fiber optics which also supplies white light to the sample. The dependence of the backreflected light on the optical wavelength is used to determine the film thickness. OFTM has the advantage that the thickness, the refractive index and the roughness of the BCP thin film can be determined continuously during SVA. From the film thickness, the volume fraction of the solvent can be determined, assuming that the increase in film thickness is entirely due to solvent uptake.

3.2.2. Chambers based on a flow of solvent vapor

For accessing lower organic vapor pressures, for instance for materials that dewet from the substrate upon too high a degree of swelling, the bubbler method is more suitable. The chamber described in Ref. [141] is shown schematically in Fig. 7a. Several versions of this type of chamber were developed by us. In the first version, a flow meter located outside the experimental hutch was connected to the gas supply (typically 1 bar) by a long tube. After the flowmeter, the gas line was split into two, one part being connected directly to the chamber and the other to the bubbler, a flask of volume 100 ml which contained 60 ml of liquid solvent. These two gas flows were controlled by magnetic valves. The exit line of the bubbler was connected to a three-way valve which allowed installing the desired gas flow (typically ~0.4 l/h or ~1.2 l/h) and making sure it was stable before directing the flow to the sample chamber, which defined the beginning of SVA. The sample was typically kept in vapor for 45 min, and then it was

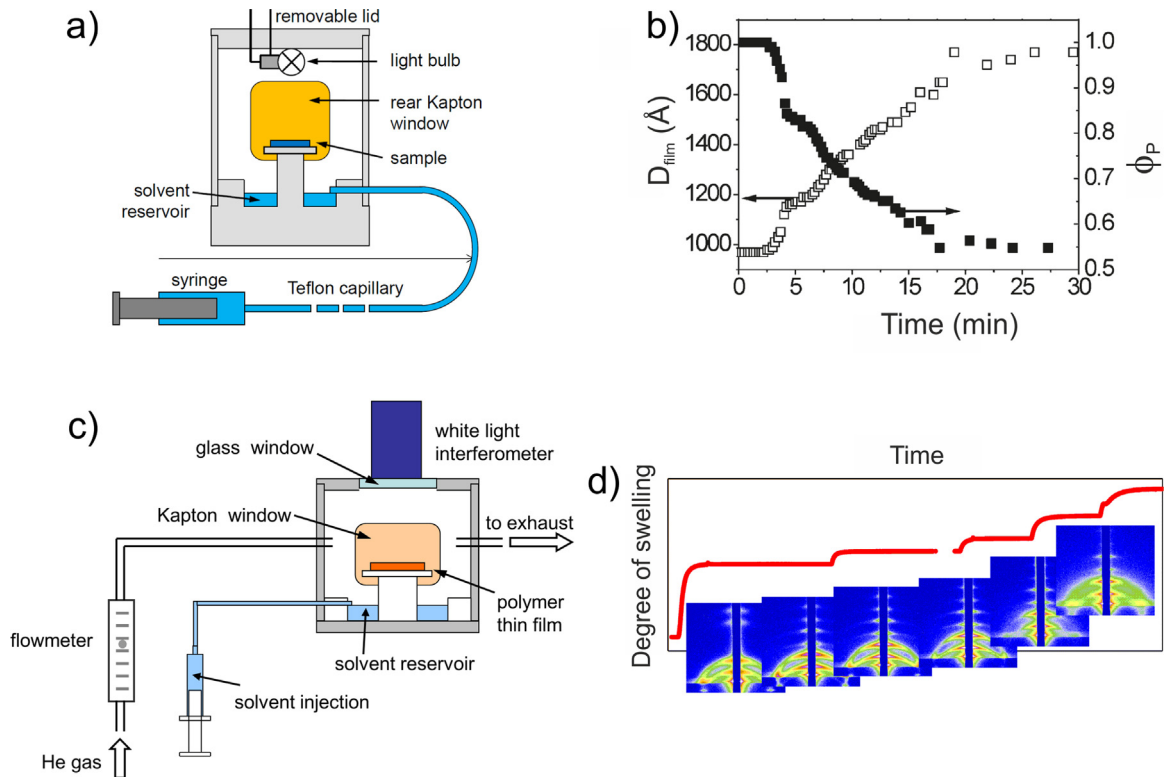


Fig. 5. Sample chambers for in situ GISAXS during SVA. (a) Chamber using liquid solvent without a gas flow. (b) Corresponding film thickness of a PS-*b*-PB thin film, D_{film} (left axis) and corresponding polymer volume fraction, ϕ (right axis). (c) Chamber using liquid solvent and a gas flow. (d) Corresponding film thickness profile and representative GISAXS images of a PS-*b*-PB thin film.
Sources: (a) Own figure. (b) [120]. Copyright 2010. Reproduced with permission from the American Chemical Society. (c) and (d) [111]. Copyright 2012. Reproduced with permission from the American Chemical Society.

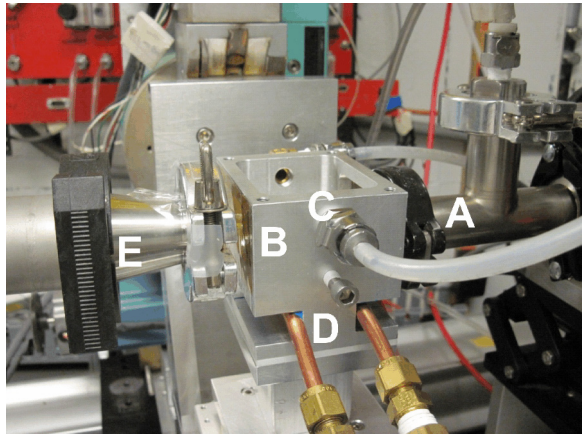


Fig. 6. Photograph of the CHESS D1 SVA chamber. A incident flightpath, B chamber, C gas inlet (top) and liquid inlet (bottom), D chamber temperature control, E exit flightpath. The lid with integrated OFTM was removed. The X-ray beam direction is from right to left. The chamber can be used with liquid solvent in the cell or with a bubbler.

dried for about the same time at a N_2 flow rate of the same magnitude.

Since the drying process is very fast when switching from vapor to dry gas, in a second version of the vapor control system, the magnetic valves were replaced by

proportional valves which allowed controlling the swelling and the drying rate much more precisely. In addition, the sample chamber was equipped with two separate inlets to avoid backflow in the tubes. Similar flow rates as before were typically used. Drying was achieved by keeping the vapor flow through the bubbler constant and unchanged from the swelling process, while the flow of pure N_2 gas was increased step by step from zero to $\sim 3 \text{ l/h}$ within 50 min. Afterwards, the solvent vapor flow was decreased step by step to zero within 25 min. This resulted in slow, linear deswelling of the BCP thin film [121,139]. In the latest version, the proportional valves have been replaced by computer-controlled mass flow controllers. Using programmed macros, the reproducibility of the SVA procedure was ensured. This way, nearly linear swelling and deswelling of the films were achieved over typically 40–50 min (Fig. 7b).

The chamber described by Gu et al. [138,140] features Kapton windows for the X-ray beam and a quartz window on the chamber top for the OFTM similar to the chambers described above. Solvent vapor is introduced from a bubbler into the chamber using inert gas as a carrier gas. In contrast to the procedure described above, dry inert gas and solvent-rich gas are mixed prior to flowing into the chamber, i.e. the total vapor pressure and the partial pressure of the solvent vapor in the chamber can be controlled by the relative flow rates (Fig. 7c). Drying of the film is

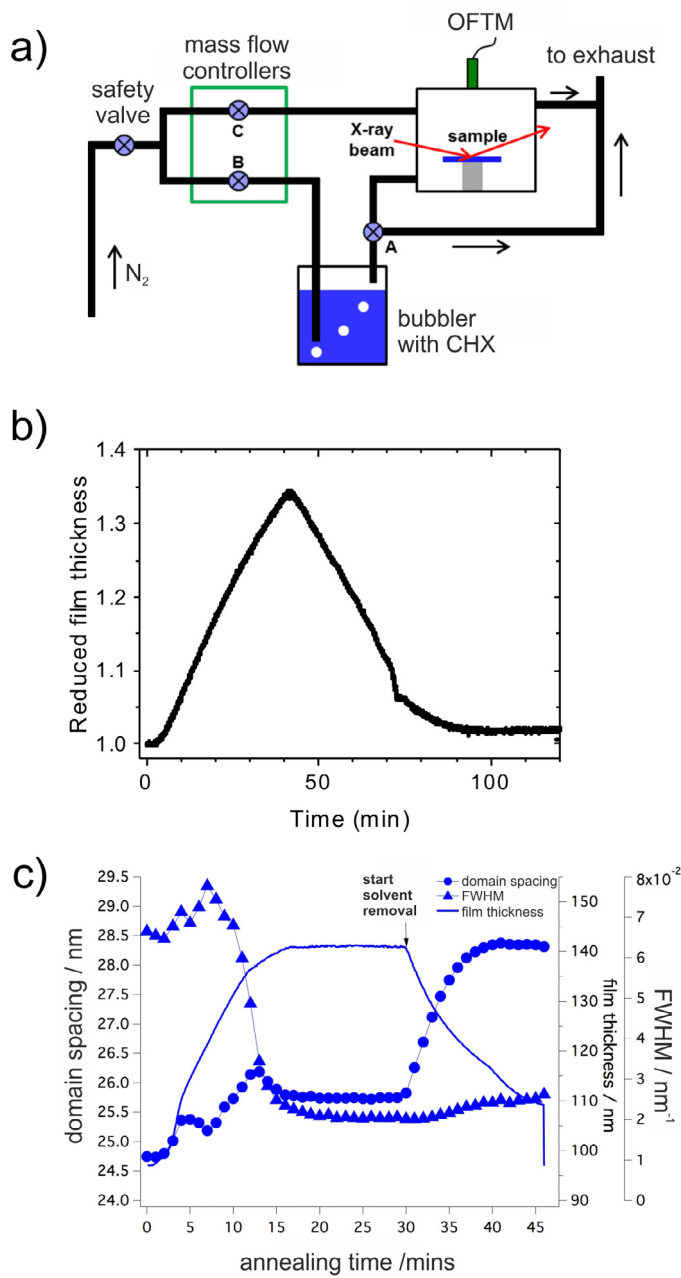


Fig. 7. Sample chambers based on a flow of solvent vapor. (a) Schematics of chamber. (b) Corresponding reduced film thickness (i.e. normalized to the dry film thickness) as a function of treatment time. Thickness data from OFTM of a PS-*b*-PB thin film [139]. (c) Results from a similar chamber described in Ref. [140]: Film thickness (solid line) of a PS-*b*-P2VP thin film from OFTM, as well as repeat distance (circles) and FWHM of Bragg reflection (triangles) from GISAXS, all vs. annealing time.

Source: (a) [141], Copyright 2014. Reproduced with permission from John Wiley and Sons. (c) [140], Copyright 2014. Reproduced with permission from Springer.

accomplished by closing the vapor inlet and purging the chamber with pure inert gas. Controlling the flow rate of the inert gas allows control and variation of the removal of solvent vapor from the chamber. Flow rates during drying varied from 10 to 50 sccm [138,140].

The vapor build-up in the chamber under ambient conditions is controlled by diffusion and/or flow-induced

mixing [146]. For typical cells with a volume of 100–200 mL, the time constant is around 3–5 min for a step-like change, e.g., liquid injection or opening a valve for solvent-containing gas flow. As long as mass flow controllers work on the same time scale, well-defined vapor concentration profiles can be obtained (see Fig. 7b). However, intrinsic polymer kinetics may be on a faster time

scale. If fast solvent removal during evaporation is aimed for together with real-time GISAXS studies in order to follow such fast reorganizations, two conditions must be fulfilled: (i) A controlled and fast solvent evaporation has to be achieved, and (ii) sufficiently fast GISAXS measurements must be possible. Fast solvent removal during evaporation can be achieved by opening the lid of the cell, providing a large cross section for the vapor to escape. Alternatively, the cell could be evacuated or a large purge flow used. If the opening of the cell or its evacuation can be automated, such fast evaporation could be studied in detail with the new generation of pixel array detectors (see Section 3.3). Modern synchrotron sources provide the required flux. In our own experience, most features of the scattering image for PS-*b*-PB can already be discerned in 0.1 s when the incidence angle is chosen to be between the film and substrate critical angles.

3.3. GISAXS experiments

The typical setup for a GISAXS experiment (Fig. 8) includes an X-ray source and a collimating section, similar to transmission SAXS. For ex situ measurements and in situ equilibrium studies, a lab source is in many cases sufficient, whereas for time-resolved investigations, a high-flux source, i.e. synchrotron radiation, is mandatory. By now, dedicated GISAXS set-ups are available at most synchrotron sources [54]. Both bending magnet and insertion device beamlines are available. The use of multilayer optics has been highly beneficial at bending magnet beamlines [147], increasing the flux due to the higher bandwidth compared to a silicon monochromator without compromising the resolution [148].

The sample is positioned on a precision goniometer which provides typically three rotations – sample azimuth, sample tilt, and incident angle of the beam. The sample azimuth motion rotates the sample around its surface normal and is mainly used to study laterally anisotropic samples. The sample tilt allows placing the sample parallel to the pixel rows of the detector and also keeps the sample positioned in the beam, when multiple lateral positions are probed. Two translations, sample height and sample position perpendicular to the beam complete the sample stage; the former is critical to sample line-up, the latter is used to probe different parts of the sample. Typical incident angles for organic thin films on silicon wafers are between the critical angles for total reflection of the film and the silicon substrate, corresponding to $\sim 0.1^\circ$ and $\sim 0.2^\circ$, respectively, at a photon energy of 10 keV, i.e. with this choice of incident angles, the beam penetrates the sample but is reflected off the substrate. Under these conditions, the sample volume is fully illuminated along the footprint of the beam. At a typical vertical beam width of 0.1 mm and an incident angle of 0.2° , the footprint is on the order of 30 mm in length. The horizontal beam width is typically 0.5 mm which yields a strong signal at the detector without compromising resolution. Finally, inclusion of a fast shutter admits the beam to strike the sample only when either lining up or taking scattering images. Thus, radiation-sensitive organic samples are well protected from unintended exposure.

An exit flight path, either evacuated or filled with helium, is installed to reduce both attenuation of the beam and air scattering. The detector is protected from the intense specular and diffuse reflectivity in the incident plane [149] with a 2–3 mm diameter metal rod, which ensures that the weaker GISAXS signals scattered out of the incident plane are accessible for detection. In other cases, two independent disk-like beamstops protect the 2D detector from the incident and the reflected beam, but allow detecting the diffuse scattering signal in the plane of incidence (Fig. 8) – in some cases, crucial information can be hidden behind a rod-shaped beamstop [139]. The sample-detector distance chosen depends on the length scales to be probed and may range from ~ 0.5 m to 2 m for nanoparticles and block copolymers (3–100 nm resolution) and up to ~ 10 m for GIUSAXS with resolution ranging into the micron range [150].

X-ray area detectors of various types (CCD: MedOptics, MAR, Princeton Roper; pixel array detectors: Pilatus series from Dectris) are typically used. Background, flat field, and distortion corrections [151] of the detector raw images are often carried out automatically. The read-out time of the CCD images of a few seconds together with the acquisition time necessary to obtain reasonable statistics (typically 1–10 s, depending on the system investigated and the available photon flux) limits the investigation of fast kinetics. Moreover, CCD cameras feature an intrinsic background, so-called read-out noise, which limits the sensitivity of the detector and which has to be taken care of in the data analysis. Recently, pixel array detectors have become commercially available (Dectris) and proven useful for experiments where fast kinetics and/or very low background are required, such as the ordering processes in conjugated polymers and molecules [152]. Such detectors can record up to 100 images per second and do not require post-processing of image data other than what is built into the detector software. For most block copolymer studies done so far, the more limited time resolution of CCD cameras has proven to be sufficient.

The sample is usually placed horizontally on a support in the sample chamber and is aligned with alternating height and rocking scans (i.e. variation of the incident angle) using an ion chamber or a photodiode in the beamstop, while the area detector is shielded from radiation. Height scans at two lateral positions near the sample edges allow adjusting the tilt of the sample precisely. Further fine adjustment of the incident angle may be done by varying the incident angle such that the specularly reflected beam hits the detector at a certain height above the direct beam. A more refined procedure uses a reflectivity scan as a second line-up step which covers the critical angles of film and substrate employing the line-up detector. This method is specifically important for identifying the wave-guide resonances between the critical angles [153]. In addition, X-ray reflectivity information can be obtained.

Static measurements before and after SVA are often carried out using an incident angle series in the range of 0.05 – 0.30° and longer measuring times than during SVA, if possible. When an angle providing suitable signal is identified, SVA is carried out at this fixed incident angle. At this, beam damage must be prevented, e.g., by exposing

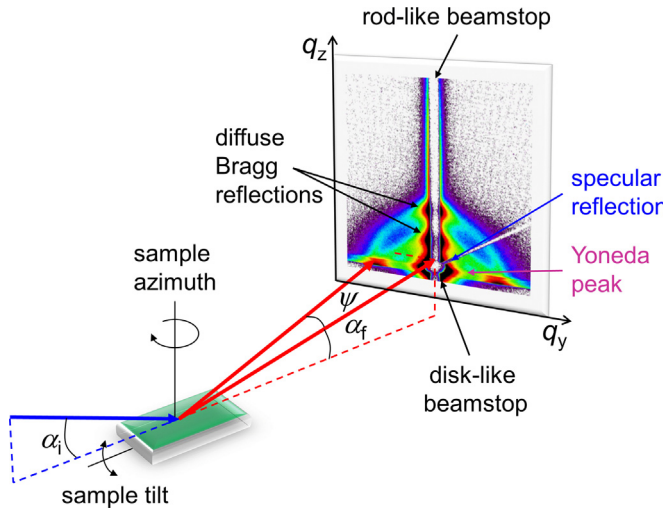


Fig. 8. Schematics of a GISAXS experiment. α_i , α_f and ψ denote the incident, the in-plane and the out-of-plane exit angle, respectively. The sample azimuth and the sample tilt are indicated. The specular reflection and the Yoneda peak are marked as well as the diffuse Bragg sheets from the thin film structure (parallel lamellae). In this case, a rod-like and a disk-like beamstop were used simultaneously. Courtesy of A. Sepe.

spots which have not been used for alignment or test measurements and by moving the sample sideward after each measurement. It is also helpful to use as small an incident angle as possible to achieve a large scattering volume and to keep the X-ray dose per second and square millimeter as low as possible.

3.4. Interpretation of 2D GISAXS maps for lamellar systems

In this section, we introduce the basic features of GISAXS. For more detailed descriptions of the scattering theory, we refer to recent reviews [49–55].

Compared to thin film studies using SAXS in transmission geometry, absorption of the beam by the substrate is avoided in GISAXS, a larger sample volume is illuminated and more structural information can be obtained in a single 2D GISAXS map than obtained with SAXS. Specifically, GISAXS probes the film structure both parallel and perpendicular to the substrate in a single measurement. The scattering vector components are defined in terms of the scattering angles (Fig. 8) as

$$\begin{aligned} q_x &= k_0(\cos \psi \cos \alpha_f - \cos \alpha_i) \\ q_y &= k_0(\sin \psi \cos \alpha_f) \\ q_z &= k_0(\sin \alpha_i + \sin \alpha_f) \end{aligned} \quad (1)$$

and $k_0 = 2\pi/\lambda$ is the vacuum wave vector of the X-ray beam of wavelength λ . α_i and α_f are the incident and exit angles, and ψ is the scattering angle in the film plane. The lateral scattering vector, $q_{||} = \sqrt{q_x^2 + q_y^2}$, is approximately equal to q_y as q_x is much smaller than q_y except close to the beamstop. Thus, scattering along q_y and q_z reveal the lateral and perpendicular structure in the sample, respectively.

The scattering parallel to the surface can be interpreted by standard SAXS scattering theory, i.e. the kinematic form and structure factors [154,155]. With regard to scattering perpendicular to the substrate, three regimes can be

distinguished as defined by the critical angles of total external reflection of polymer film, α_{cP} , and substrate, α_{cS} .

Evanescence regime: $\alpha_i < \alpha_{cP}$. In this case, the incident wave is totally reflected at the air-polymer interface, and only a damped wavefield, i.e. an evanescent wave, penetrates into the film. The penetration depth is a function of the incident angle α_i and the X-ray refractive index of the film $n = 1 - \delta$, where the dispersion δ is typically 10^{-6} [156]. For polymer films, absorption can be neglected. The penetration depth assumes a limiting value of ~ 5 nm at about a quarter of the critical angle of the polymer, and thus, near surface information of the film can be obtained at $\alpha_i \approx \alpha_{cP}/4$. As long as the penetration depth remains smaller than the film thickness, information of the film morphology averaged over a near-surface layer can be collected.

Dynamic regime: $\alpha_{cP} < \alpha_i < \alpha_{cS}$. Interpretation of scattering images taken in the dynamic regimes requires full use of the DWBA scattering theory [153,157,158]. In BCP thin films, α_{cP} is usually smaller than α_{cS} , as the electron density in organic materials is in most cases lower than in solid substrates such as silicon or glass. In this regime, it is important to consider both the refraction of the X-ray beam when it enters or exits the polymer film as well as the reflection of the X-ray beam by the substrate surface. Specifically, the reflected beam can give rise to doubling of diffraction spots in this angle regime (Fig. 9b,c) which, for parallel lamellae, is given by the two roots in Eq. (2) [155]:

$$q_z = k_{iz} + \sqrt{k_{cP}^2 + \left[\frac{2\pi m}{D} \pm \sqrt{k_{iz}^2 - k_{cP}^2} \right]^2} \quad (2)$$

where $k_{iz} = k_0 \sin \alpha_i$ and $k_{cP} = k_0 \sin \alpha_{cP}$. D is the repeat distance (lamellar thickness) and m the order of the reflection. This equation has two roots for each order; the ‘minus branch (M)’ and ‘plus branch (P)’ (Fig. 9b) corresponding to the scattering of the direct beam and the beam reflected from the substrate. The positions of the peaks along q_z vary with α_i . Fitting the peak positions in an angle series

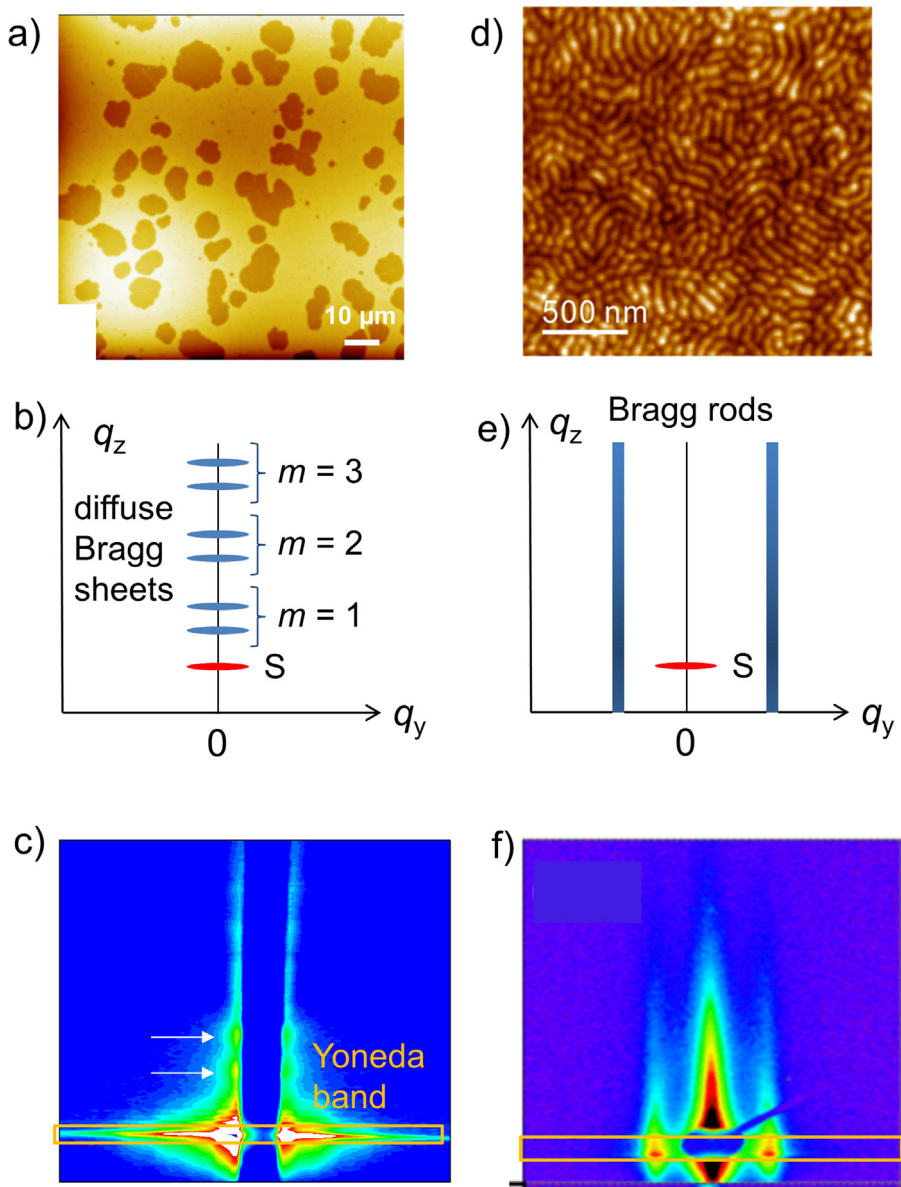


Fig. 9. Characterization of lamellar PS-*b*-PB thin films. Left: parallel lamellar orientation, $D_{\text{lam}} = 19.7 \text{ nm}$, $D_{\text{film}} = 157 \text{ nm}$. Right: perpendicular lamellar orientation, $D_{\text{lam}} = 86.0 \text{ nm}$, $D_{\text{film}} = 160 \text{ nm}$. (a,d) AFM height images, the scale bars are given in the images; (b,e) schematic GISAXS maps, m denotes the order of the DBSs and S the specularly reflected beam; (c,f) measured GISAXS maps, the orange rectangles indicate the Yoneda band between α_{cp} and α_{cs} , and the arrows indicate the positions of the DBSs.
Source: (a) and (d) [162], Copyright 2003. Reproduced with permission from the American Chemical Society. (c) [149], Copyright 2007. Reprinted with permission from the American Chemical Society. (f) [139], Copyright 2013. Reproduced with permission from John Wiley and Sons.

of GISAXS maps with Eq. (2) provides an accurate lamellar thickness D as well as the critical angle of the BCP [120,154,159].

Quasi-kinematic regime: $\alpha_i > \alpha_{cs}$. When the incident angle is larger than the critical angle of the substrate, the reflected signal drops sharply. Already at $5/4 \alpha_{cs}$, the reflected wave is weaker than 10% of the incident wave, i.e. the reflected wave will not give rise to significant interference effects. In this angle regime, the refraction of the wave when entering the film still needs to be considered for obtaining precise repeat distances in the vertical

direction. The scattering images still feature the dynamic enhancement at the Yoneda band at exit angles between the two critical angles; apart from this, the modeling of the scattered intensity can be much simplified [51,160,161]. Ultimately, it is a function of the available scattering intensity and the specific structure investigated which of the three scattering regimes is chosen.

Fig. 9 explains how information is obtained about the film mesostructure for two films featuring either parallel or perpendicular lamellae. Fig. 9a shows a measured AFM image of a DBCP film with parallel lamellae, which features

surface terraces. The periodic structure along the film normal gives rise to a series of intensity enhancements, DBSs [155], along q_z with their positions given by Eq. (2) (Fig. 9b). In Fig. 9c, the corresponding experimental GISAXS map is shown. The gray area in the middle is due to the rod-shaped beamstop. Above the specularly reflected beam, arrows indicate the positions of the DBSs.

In the case of lamellae perpendicular to the film substrate, the AFM image shows a fingerprint pattern (Fig. 9d). For such samples, that have an isotropic distribution of lamellar orientations around the surface normal and may be called 2D powders, a single GISAXS image provides full information about the sample properties both in the lateral and normal directions [143]. This structure results in BRs [155] extended along q_z and positioned at $q_y = 2\pi/D_{\text{lam}}$ (Fig. 9e,f). For a well-ordered film, higher order BRs occur. The intensity variation along the BRs can contain information on the height distribution of the domains, such as protrusions [139]. If the film contains tilted and randomly oriented lamellae, the GISAXS map shows full or partial Debye-Scherrer rings centered around the direct beam and around the reflected beam, respectively [111,120,121,155,163].

The main results of analyzing the intensity distribution in the GISAXS maps are the orientation of BCP domains in the film together with the characteristic repeat distance of the domains. In the case of lamellae, peak widths give information about the lamellar correlation as well as about undulations of the lamellar interfaces [111,120,121]. The description above is for lamellar phases, but similar analysis can be made with other morphologies, e.g., hexagonally packed lying [154,164–166] and standing cylinders [167,168], hexagonally perforated layers [154,164,165], the gyroid structure [154,165] as well as spheres forming a body-centered cubic lattice [144,169]. GISAXS maps from different morphologies have been compiled in Ref. [51]. By now, all known morphologies of DBCP thin films have been investigated with GISAXS with the aim of revealing details of the mesoscopic structures, both normal to the surface and laterally, as well as preferential alignment effects induced by the interfaces, see for instance Refs. [16,26,143,154,159,164,169–175] and the examples given in Section 4.

Dedicated GISAXS beamlines or scattering beamlines with a GISAXS option are available at most synchrotron sources around the globe at the time of writing. A listing is provided in Ref. [176]. Some excellent tutorials on GISAXS are available on the web. The GISAXS/GIWAXS tutorial by Smilgies provides an overview of basic GISAXS properties and application areas including an extensive list of references [177]. The GISAXS tutorial by Meyer provides an introduction to the scattering theory [178] and application examples. The IsGISAXS tutorial by Lazzari [179] gives a detailed account of the scattering theory and modeling. A wiki-style GISAXS page is in development at [180].

Several software packages have been developed for both data correction and reduction, including FIT2D [181], DPDAK [182], as well as Actionjava [183]. For time-resolved GISAXS, partially automated treatment and analysis is often required to handle the large amount of data obtained within relatively short experimental times.

For indexing of GISAXS patterns, NANOCELL [184] has been available for some time and is widely used [185]. The classic modeling program for GISAXS intensities is IsGISAXS by Lazzari [157,179]. Recently, other packages have been published and are freely available: FitGISAXS [158], BornAgain [186], and HipGISAXS [187].

4. Results from experiments

Complementary to ex situ investigations before and after the SVA process (many of these studies have been reviewed in Refs. [46,48]), in situ SVA and GISAXS studies of BCP thin films have aimed at studying pathways and kinetics for (i) improving the lateral order, (ii) controlling/altering the orientation of the morphology or (iii) controlling the morphology. In situ studies provide more detailed insight into the pathways of the transformations and can detect transient structures present at a certain degree of swelling. This knowledge facilitates a more efficient tuning of the SVA parameters. Results from such studies are presented in the first three sections in the following. In addition, real-time in situ investigations using GISAXS can give detailed insight regarding transition processes and mechanisms together with the relevant time scales and kinetics during SVA, and a number of key parameters have been identified during swelling and recently also during drying. This way, the underlying physical processes can be understood in conjunction with theoretical modeling. These real-time, in situ GISAXS studies addressing the mechanisms of restructuring processes in BCP thin films during SVA are described in the fourth subsection.

4.1. Studies aiming at improving the lateral order

Controlling the lateral order of the BCP microdomains (i.e. in the film plane) is in many cases essential to create templates and scaffolds for the fabrication of nanostructured materials. In pioneering work using transmission SAXS on ca. 1 mm thick lamellar and cylindrical roll-cast films of PS-*b*-PB-*b*-PS triblock copolymers, Albalak et al. [188] established that SVA resulted in similar structures and similar improved degree of lateral order as upon thermal annealing but in a shorter time. This was observed both for selective (toluene) and non-selective solvents (MEK and hexane) and was attributed to stress relaxation on the molecular level: the mobility of the glassy polystyrene blocks is enhanced upon solvent uptake which allows for relaxation of the stress from the fabrication process as well as for a repositioning of the PB/PS junctions along the interfaces. This way, volume changes when taking up solvent can be accommodated. The authors pointed out that a thorough understanding of the swelling and deswelling kinetics could be used to tailor a specific response of a BCP to solvent exposure.

On thin films prepared by spin or dip coating or by drop-casting, a number of ex situ investigations have been carried out before and after SVA using imaging methods, such as AFM and TEM [189–191]. These studies give valuable local structural information, but only indirect hints to the pathways of structure improvement. Moreover, these experiments can be tedious in some cases because staining

Table 1

Results from in situ GISAXS investigations aiming at improving the lateral order.

| Author/reference | Polymer | Solvent | Resulting morphology |
|-----------------------|--|---------|----------------------|
| Kim et al. [128,192] | PS- <i>b</i> -PEO with different salts | Benzene | Standing cylinders |
| Cavicchi et al. [129] | PI- <i>b</i> -PLA | Benzene | Lying cylinders |

or etching may be needed to create contrast, and a large scanning area is needed to obtain good statistically averaged information; thus, the identification of suitable SVA parameters is not straightforward.

The importance of in situ GISAXS studies to characterize the appearance of long-range order in BCP thin films was demonstrated in several investigations [128,129,192]. The results are compiled in Table 1. We have shown [143] that lamellar structures of 75 nm period could be resolved in grazing-incidence scattering geometry. In addition, our preliminary real-time, in situ data showed that changes in block copolymer morphology can be traced on a convenient time-scale of minutes [143]. Combining AFM and real-time in situ GISAXS during drying, Kim et al. [128] demonstrated that, in PS-*b*-PEO thin films, nearly defect-free arrays of standing cylinders with long-range lateral order can be formed by SVA in benzene, a good solvent for both blocks. The authors proposed that evaporation of the solvent at the free surface leads to an ordering front which propagates through the entire film, i.e. the ordering process is analogous to zone refining. These results are in accordance with theoretical predictions [103]. In a later paper, the authors investigated in situ the effect of the presence of salts of different kinds in thin films from the same cylinder-forming PS-*b*-PEO DBCP, where the salt formed complexes with the PEO block. They found that by increasing the salt content, the long-range order is significantly enhanced during SVA with benzene [192]. The GISAXS maps taken in situ during swelling and drying showed that a thin film containing a low amount of salt only formed standing cylinders during drying (Fig. 10a), whereas a thin film containing a high amount of salt became highly ordered already in the swollen state (Fig. 10b). Using metal salts, functioning as nanoparticle precursors, highly ordered, functional and self-orienting systems could be created [192].

Cavicchi et al. carried out an in situ GISAXS investigation during SVA on thin films from PI-*b*-PLA DBCPs using benzene, which is an overall good, but somewhat selective solvent toward PLA [129]. These compositionally asymmetric DBCPs formed PLA cylinders in a PI matrix and were strongly segregated, i.e. the χ parameter was high. After spin coating of Si wafers having a native oxide layer, the films (thickness ~100 nm) showed only very short-range order (Fig. 11a). Using a chamber to which liquid benzene was added by means of a syringe and treating the DBCP thin film for 1–30 min, the cylinders' defect density was strongly reduced (Fig. 11c). (If, however, the system was swelled too much, it disordered.) Using AFM, lying cylinders were observed after drying which was achieved by slowly flushing the cell with dry N₂ gas (Fig. 11c). In situ GISAXS in the swollen state using a chamber similar to the one in Fig. 5c revealed lying cylinders (Fig. 11b) which became even better stacked along the film normal after slow drying (Fig. 11d).

4.2. Studies aiming at controlling the orientation of the morphology

A number of studies have demonstrated that not only the degree of long-range order can be improved by SVA, but also the orientation of the microdomains may be altered. In an early work, Fukunaga et al. [190,191] investigated thin films of lamellae forming PS-*b*-P2VP-*b*-PtBMA triblock copolymers by ex situ AFM and TEM. They found that slow solvent extraction lead to parallel lamellar microdomains whereas fast drying resulted in perpendicular lamellae which were aligned over large lateral areas. The authors explained this dependence by the mechanical strain fields present during the drying process.

Morphological changes were first observed in situ by Cavicchi et al. who investigated a cylinder-forming PI-*b*-PLA DBCP similar to the one described in Section 4.1 [129,167]. Using chloroform for SVA, a solvent good for both blocks, but slightly more selective for the cylinder block PLA than benzene (which just resulted in an improved degree of order of the lying cylinders, see Section 4.1), standing cylinders were observed, which were preserved during drying. The authors attributed these findings to the fact that both solvents increase the polymer mobility, but chloroform additionally mediates the interfacial interactions in the film sufficiently, such that preferential segregation of one block to the surface was prevented, and the commensurability between the film thickness and the repeat distance becomes the dominating control parameter. In this study, the structural information from in situ GISAXS was used to monitor the microdomain orientation during SVA, while nothing was inferred about the pathway of restructuring of the polymers taking place during swelling and drying. The findings are compiled with those from the studies discussed below in Table 2.

Paik et al. [144] investigated a thin spin coated film of compositionally asymmetric PoMS-*b*-PHOST which was found to form standing PoMS cylinders in a PHOST matrix. The film was significantly thicker than the repeat distance of the morphology. In the as-prepared thin film, it featured only short-range order. The film was swollen with THF, a good solvent for both blocks, which was injected into the sample chamber in the liquid state while controlling the degree of swelling of the film by a flow of inert gas. In situ GISAXS measurements (Fig. 12) revealed that the Bragg rods due to standing cylinders vanished at a certain degree of swelling and that, upon further swelling, Bragg reflections from parallel cylinders appeared (compare Fig. 12a and 12d). Upon solvent evaporation, the parallel cylinder orientation persisted (Fig. 12e). From the appearance of the new set of Bragg reflections at the expense of the initial ones and the absence of a Debye–Scherrer ring (which would signify a random cylinder orientation), the authors concluded that the standing cylinders coalesce

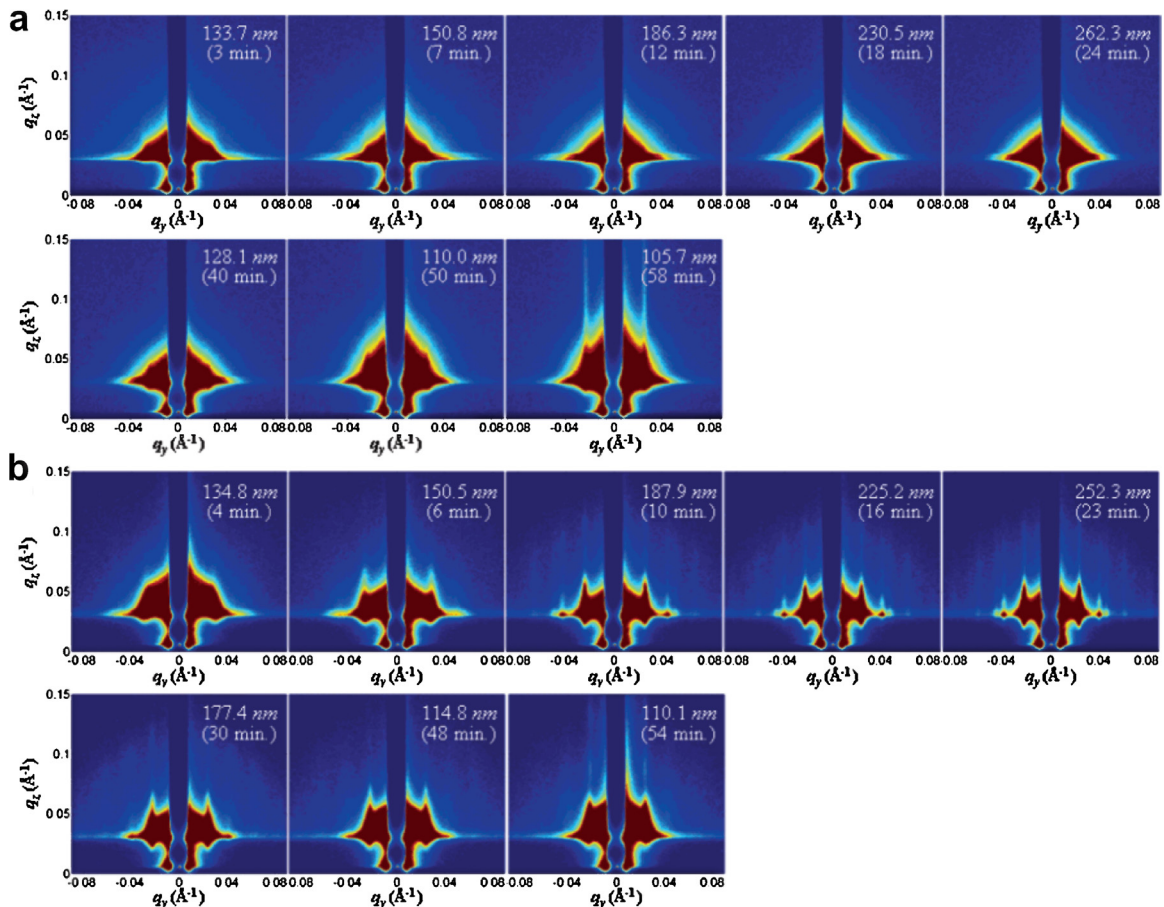


Fig. 10. GISAXS maps from cylinder-forming PS-*b*-PEO thin films containing a low (a) and a high salt content (b). In each case, the maps in the top and bottom rows are taken during swelling with benzene vapor and during drying, respectively. The film thicknesses and the times are indicated in the maps. Source: [192]. Copyright 2006. Reproduced with permission from the American Chemical Society.

Table 2

Results from *in situ* GISAXS investigations aiming at controlling the orientation of the morphology.

| Author/reference | Polymer | Solvent | Initial morphology | Final morphology |
|--------------------------|--------------------------------|------------|-------------------------------------|--------------------|
| Cavicci et al. [129,167] | PI- <i>b</i> -PLA | Chloroform | Lying cylinders | Standing cylinders |
| Paik et al. [144] | P α MS- <i>b</i> -PHOST | THF | Standing cylinders | Lying cylinders |
| Gowd et al. [193,194] | PS- <i>b</i> -P4VP | Chloroform | Standing cylinders | Lying cylinders |
| Di et al. [120] | PS- <i>b</i> -PB | CHX | Parallel/randomly oriented lamellae | Parallel lamellae |

with neighboring standing cylinders to form new lying cylinders.

Gowd et al. also studied reversible orientational changes of cylinder microdomains in thin DBCP films during SVA [193,194]. The system studied was cylinder forming PS-*b*-P4VP, and the films were prepared by dip coating a specially cleaned, hydrophilic silicon wafer. The films were then annealed in 1,4-dioxane vapor, which resulted in hexagonally packed, standing P4VP cylinders in a PS matrix, as evidenced using GISAXS (Fig. 13a). For investigation of SVA *in situ* using GISAXS, these films were swollen in saturated chloroform vapor (a non-selective solvent) and dried by letting nitrogen gas into the sample chamber (Fig. 5c). GISAXS maps were recorded every 15 s (Fig. 13a–c). SVA resulted in disordering and a subsequent re-orientation of perpendicular cylinders to the parallel orientation. Fig. 13d

shows the proposed mechanism for the reorientation: during uptake of solvent, the volume fraction, f , stayed constant, since the solvent is non-selective. However, the effective Flory–Huggins interaction parameter, χ_{eff} , was lowered, and an ODT occurred. When solvent left the film during drying, the opposite process took place, and cylinders reformed within seconds. P4VP chains preferentially adsorb onto the hydrophilic silicon wafer, while PS has the lowest surface tension and thus migrates to the air-polymer interface. The result is the formation of lying P4VP cylinders in a PS matrix.

In all studies cited above [144,193,194], lying cylinders were obtained from initially standing cylinders, which was attributed to the selectivity of the substrate toward one of the blocks and the difference in surface tensions of the two blocks. Whereas in Ref. [144], the BCP thin film remained

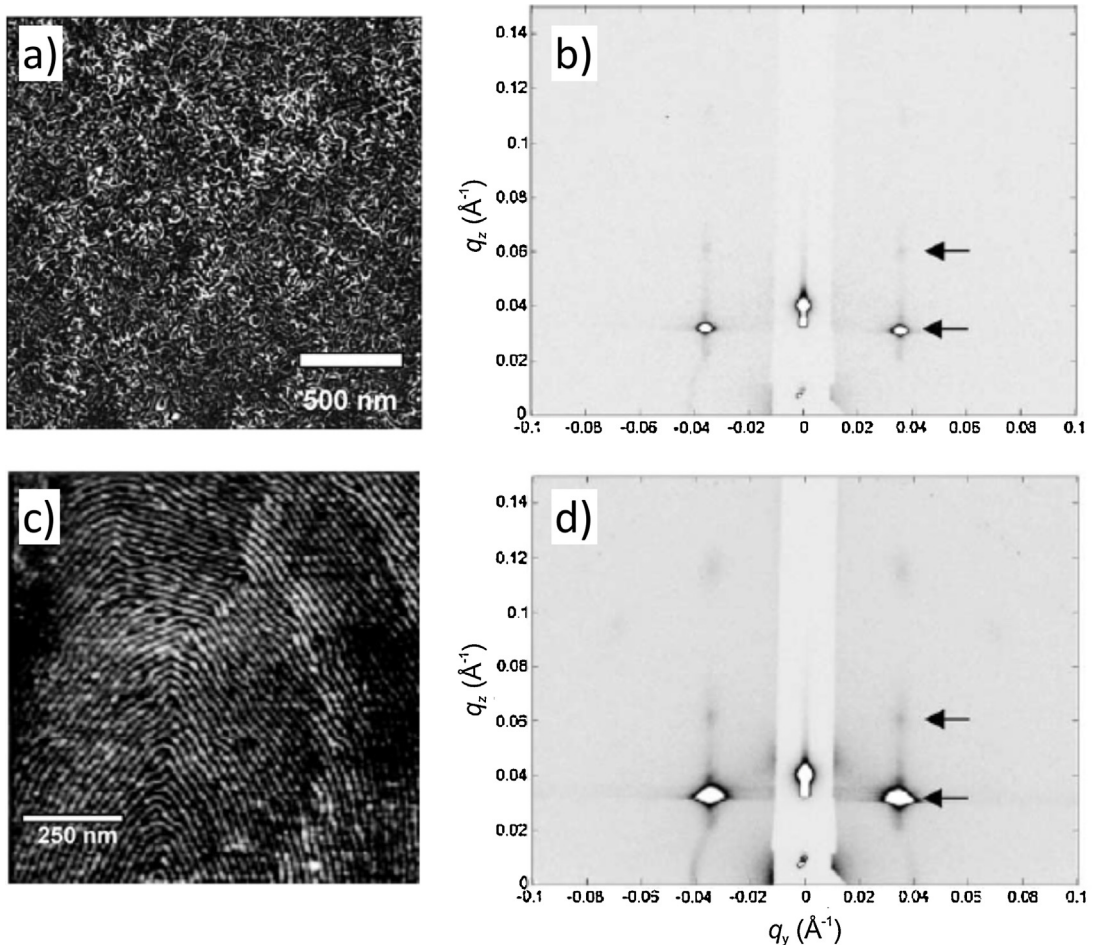


Fig. 11. Results from SVA on thin films from cylinder-forming PI-*b*-PLA. AFM images (left) and in situ GISAXS maps (right) of a PI-*b*-PLA thin film. (a) After spin coating. (b) Swollen with benzene and (c,d) after drying. The arrows indicate the Bragg reflections expected for the hexagonal lattice formed by lying cylinders.

Source: [129]. Copyright 2005. Reproduced with permission from Elsevier.

in the ordered state throughout, the film in Refs. [193,194] crossed the ODT, and the morphology reformed. In Ref. [195], lying cylinders formed in both cases.

A typical application of SVA is to improve the degree of orientational order which may be poor after spin coating. Di et al. found that SVA can transform a poorly oriented morphology into a well-oriented one [120] and confirmed this way previously obtained results of a similar system [196]. A thin film was prepared from a low molar mass, lamellar PS-*b*-PB DBCP by spin coating a UV cleaned Si wafer from toluene, a non-selective solvent. The film thickness was ca. 100 nm, i.e. ca. 5 times the lamellar thickness. GISAXS revealed that, in addition to the DBSSs expected for parallel lamellae, a Debye–Scherrer ring was present, indicating that also randomly oriented lamellae were present (Fig. 14a). SVA in a saturated atmosphere (Fig. 5a) of CHX, a solvent slightly selective for the PB block showed that the Debye–Scherrer ring vanished after a few minutes and only the DBSSs remain, i.e. the parallel lamellar orientation dominated. This was the case for a time interval 8–14 min after the injection of liquid CHX into the sample cell, which corresponds to a polymer volume fraction decreasing from

$\phi_P \cong 0.77$ to $\phi_P \cong 0.65$. For lower polymer volume fractions, the thin film became disordered. A transient state of improved lamellar order was thus encountered, which is a result of the competition between increased polymer mobility and screening of the repulsive interaction between PS and PB (Fig. 14b).

4.3. Studies aiming at altering the morphology

SVA in combination with in situ GISAXS has been shown to be able to alter the morphology of BCP thin films [144,193,194,197]. Using the same PaMS-*b*-PHOST DBCP as described in Section 4.2, but with a selective solvent (acetone), Paik et al. demonstrated a morphological transition from standing cylinders to the BCC spherical phase (Fig. 15, Table 3). Acetone is selective to the PHOST matrix, and SVA thus changes the volume fractions of the two domains [144]. Swelling by 268% with respect to the initial film thickness of 146 nm was needed to obtain sufficient chain mobility for the order–order–transition to occur, i.e. the glass transition temperature of the swollen domains must decrease below room temperature. The transition

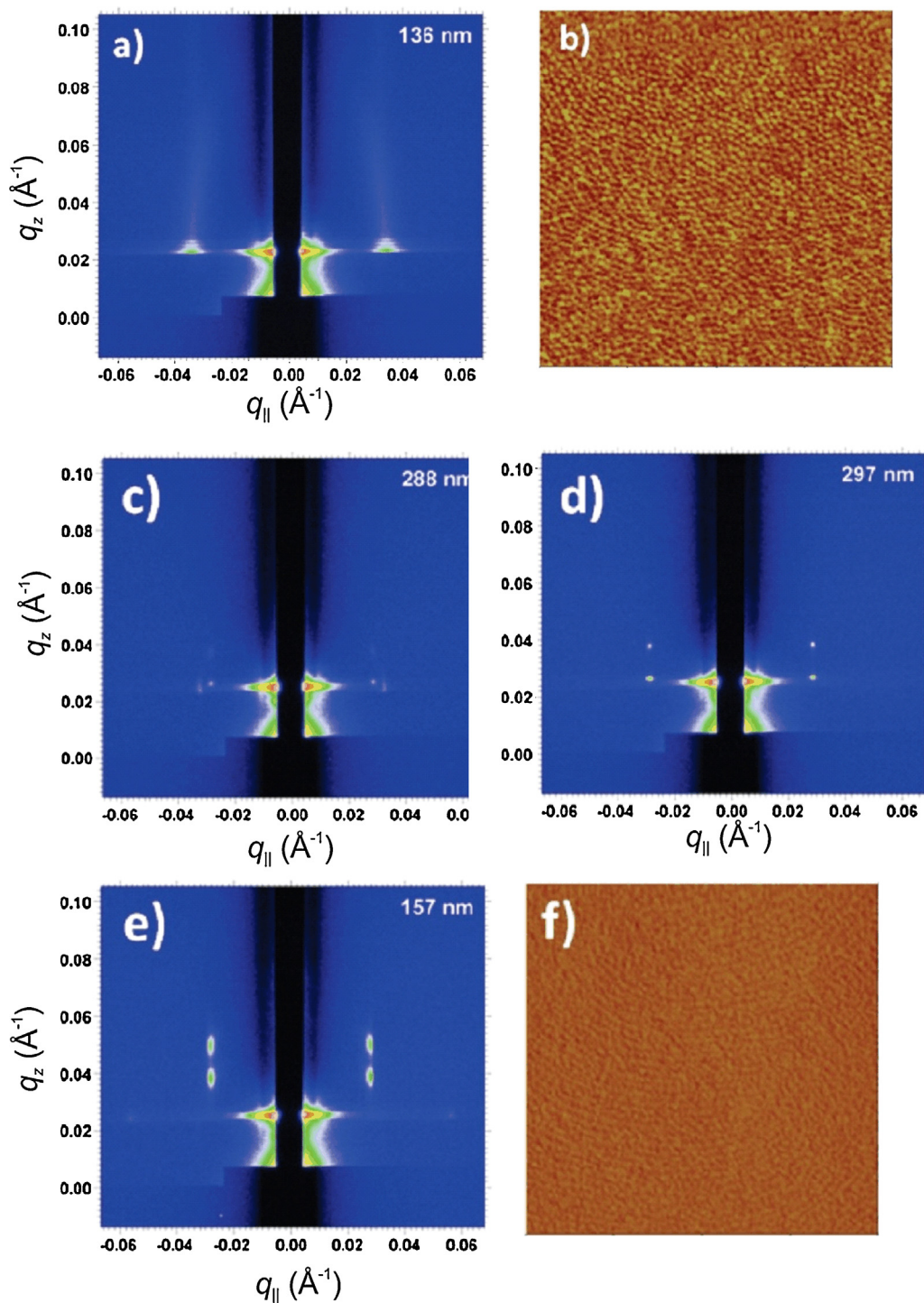


Fig. 12. In situ GISAXS 2D images (a,c-e) and AFM phase images (size 1 $\mu\text{m} \times 1 \mu\text{m}$, b,f) of a thin film from a cylinder-forming PaMS-*b*-PHOST. (a,b) as-spun, (c,d) during swelling with THF, (e,f) after drying. The film thicknesses are given in the GISAXS images.
Source: [144]. Copyright 2010. Reproduced with permission from the American Chemical Society.

was investigated using in situ GISAXS. During swelling, the Bragg rods disappeared, and rings appeared indicating prevailing of microphase separation, but a lack of orientational order. Upon further swelling, the rings transformed into

distinct Bragg reflections of the BCC morphology which was stable during 60 min at the given film thickness. The new morphology was well oriented, as could be judged from the width of the Bragg reflections. Their positions

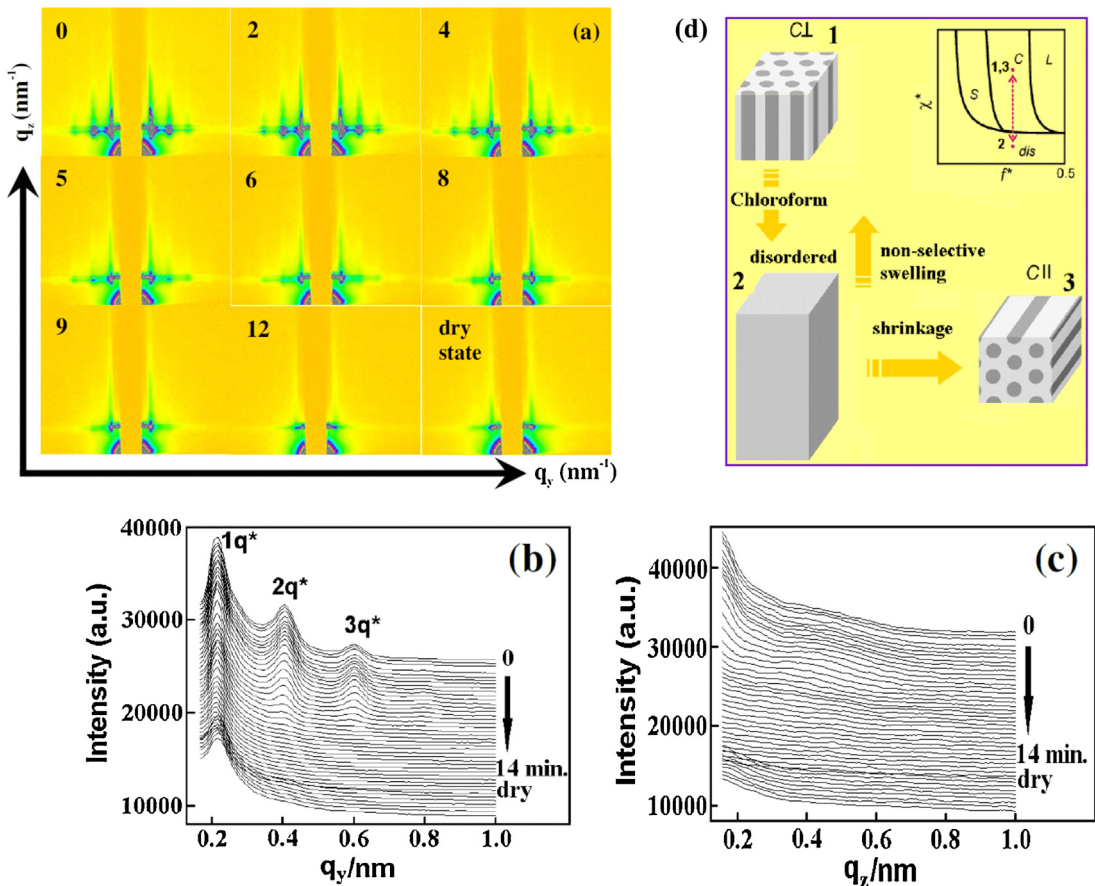


Fig. 13. Results from a PS-*b*-P4VP thin film featuring initially standing cylinders during SVA with chloroform. (a) Real-time in situ GISAXS maps during SVA using chloroform and after drying (last image). The numbers indicate the SVA time in minutes. In-plane (b) and out-of-plane intensity profiles at $q_y = 0.22 \text{ nm}^{-1}$ (c), both datasets extracted from (a). (d) Schematic representation of the re-orientational process including a schematic phase diagram. Source: [193]. Copyright 2010. Originally published under a CC BY-NC-SA licence by IOP Publishing.

Table 3

Results from in situ GISAXS investigations aiming at altering the morphology.

| Author/reference | Polymer | Solvent | Initial morphology | Final morphology |
|-----------------------|-----------------------|-------------|----------------------------|---------------------------------|
| Paik et al. [144] | PaMS- <i>b</i> -PHOST | Acetone | Standing cylinders | BCC |
| Gowd et al. [193,194] | PS- <i>b</i> -P4VP | 1,4-dioxane | Standing cylinders | BCC from ellipsoids |
| Gunkel [197] | PS- <i>b</i> -P4VP | THF | Hexagonally packed spheres | Orthorhombically packed spheres |

could be modeled as arising from a BCC lattice stretched by 6% along the film normal, i.e. in fact a face-centered orthorhombic morphology. This result showed that the lattice can swell freely along the film normal, but swelling is restricted within the film plane. Upon fast drying, the morphology stayed unchanged but both the repeat distance and the sphere radius were now compressed along the film normal compared to the bulk BCC morphology. The authors demonstrated also reversible switching of the morphologies by alternating SVA with the non-selective solvent THF and selective acetone.

Gowd et al. studied a thin film from the same PS-*b*-P4VP DBCP as described in Section 4.2 but this time, they used a solvent selective for the majority PS block (1,4-dioxane) [193,194]. In this case, the system did not disorder, but followed the mechanism outlined in Fig. 16, which involves an order-order transition (cylinder to ellipsoid). In order to

confirm the mechanism, a form factor for the discrete units was extracted from the out-of-plane GISAXS profiles while also taking polydispersity into account, and the underlying lattice was modeled as BCC with paracrystalline distortions. In this case, during swelling, both f and χ_{eff} changed (see phase diagram in Fig. 16), and the cylindrical P4VP domains changed directly into ellipsoidal domains in the swollen state. Subsequent fast drying lead to shrinkage of the film thickness and coalescence of these ellipsoids into standing cylinders when the solvent left the film rapidly along the film normal, i.e. the rate of solvent removal is important for kinetically trapping the vertical morphology.

In a recent study, Gunkel et al. [197] found an in-plane restructuring of the P4VP spheres in a PS matrix. Swelling in THF (which is selective for the PS matrix) leads to hexagonally packed microdomains. During drying, face-centered orthorhombic packing was observed in addition to the

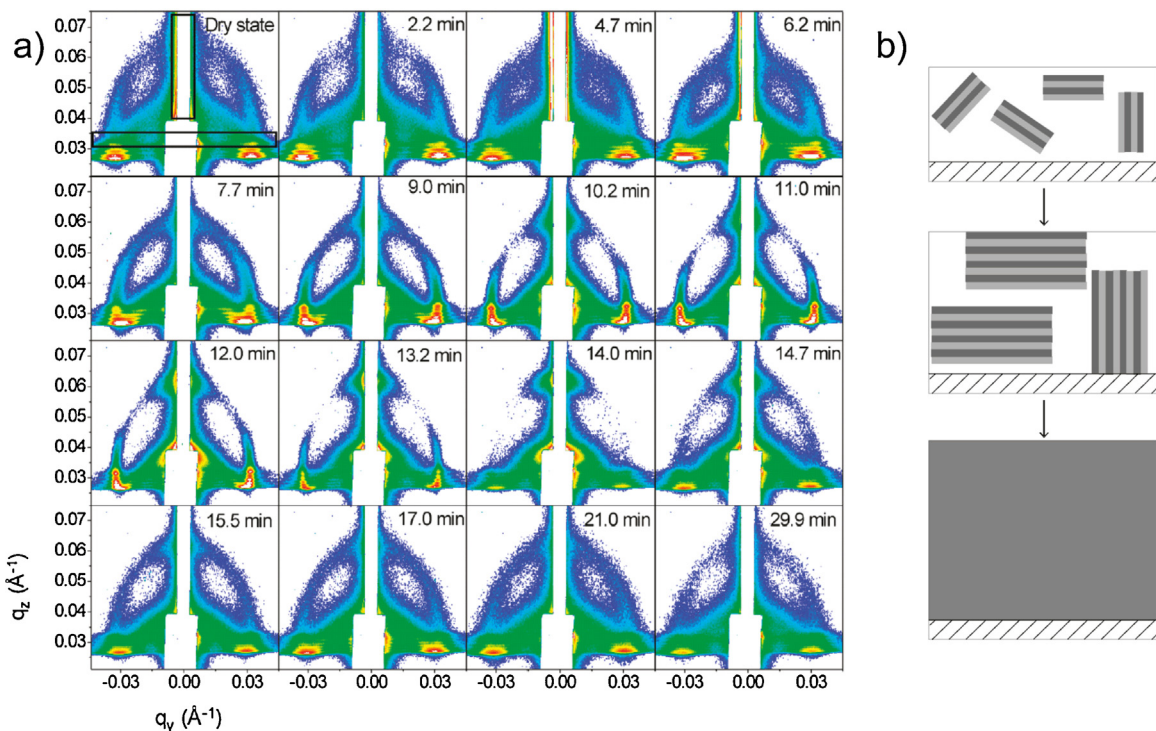


Fig. 14. Change of orientational order in a lamellar PS-*b*-PB thin film. (a) 2D GISAXS maps during swelling with saturated CHX vapor. The times after injection of solvent into the sample cell are given for each map. (b) Schematics of the corresponding structural changes.
Source: [120]. Copyright 2010. Reproduced with permission from the American Chemical Society.

hexagonal one, especially then the drying rate was low. The authors point to the difficulty of maintaining the structures obtained by swelling in a selective solvent upon drying.

Systematic investigations of the morphologies obtained upon SVA of thin films of P2VP-*b*-PDMS, a strongly segregated DBCP, were recently carried out by Jeong et al. using an ex situ sample series spun-cast on patterned substrates [133]. Applying vapors of solvents of different selectivity, allowing control of the degree of selective swelling of the matrix, the films were found to undergo morphological transitions between the initial lamellar morphology and morphologies featuring spheres, cylinders or HPL, which is of great interest for nanolithography. The morphologies were characterized after SVA, e.g. ex situ, by etching away the PDMS surface layer and the P2VP matrix and by imaging the remaining oxidized PDMS patterns using SEM. So far, no GISAXS investigations were performed on these systems; however, the work demonstrates the power of the SVA procedure in controlling BCP thin film morphology.

4.4. Real-time *in situ* studies of restructuring processes during SVA

While the majority of studies using GISAXS on thin diblock copolymer films address the structures resulting from specific treatments, a number of studies have addressed the more complex issue of the mechanisms behind the restructuring processes using real-time *in situ* GISAXS [111,120,121,129,131,134,138–140,193,194, 197–199].

Generally, during a time-resolved GISAXS experiment, a large amount of data are generated which represents a challenge in efficient screening and analysis of data. *In situ* GISAXS studies typically take advantage of implementing additional measurement techniques in order to control and monitor the process studied with multiple probes, such as thickness measurement [129,131], gravimetric measurement [200], optical micrographs [152], and imaging ellipsometry [201].

In one of the first real-time *in situ* soft matter/solvent interaction GISAXS studies, evaporation induced self-assembly in a silica/surfactant system was investigated with 10 s acquisition time and 5 s transfer time and with simultaneous gravimetric analysis [200,202]. Since then, real-time *in situ* GISAXS has been used to study a number of processes in BCP thin films, mainly related to the solvent annealing process in focus in this review. However, also other processes in BCP films have been studied, for example magnetic nanoparticle patterning (cobalt on polystyrene-*b*-block-poly(ethylene oxide), where deposition of Co was followed *in situ* with GISAXS on a 1 second time scale [203]. As described in Sections 4.1 and 4.2, Kim et al. [128] and Cavicchi et al. [129] carried out early *in situ* GISAXS investigation with some time-resolution during SVA on thin BCP films while Papadakis et al. were the first to use real-time *in situ* GISAXS to study the mechanisms of restructuring in thin BCP films [131]. The sample in this and other related studies of reorganization processes during SVA was compositionally symmetric PS-*b*-PB DBCPs [111,120,121,131,139]. Symmetric PS-*b*-PB

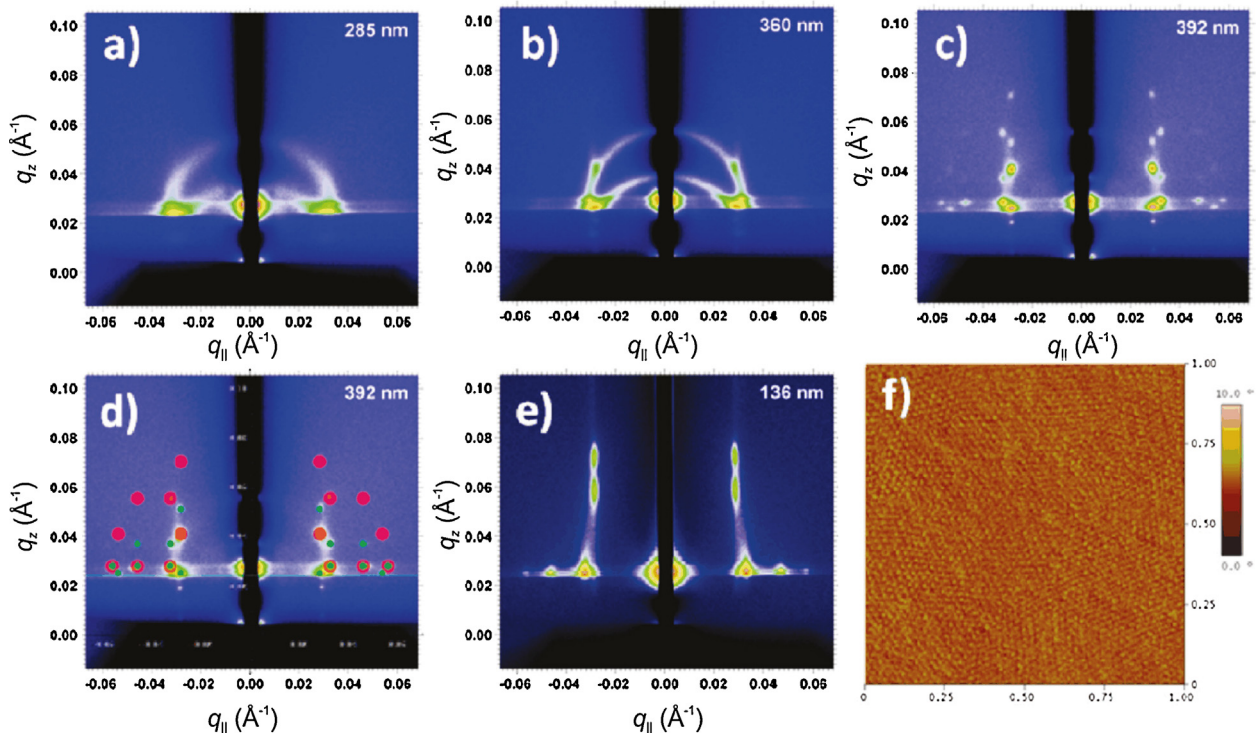


Fig. 15. SVA of a P α MS-*b*-PHOST thin film in acetone. (a–e) 2D GISAXS maps measured *in situ* and AFM image (f) of a P α MS-*b*-PHOST thin film. (a–c) Change from cylinders to spheres. (d) Scattering from the swollen, spherical film with an overlay of the modeled scattering from a stretched BCC lattice (red circles). (e) The GISAXS profile of the dried film consistent with a compressed BCC lattice. (f) AFM height image after drying. The height scale is 10 nm. (For interpretation of the references to colour in this figure legend, the reader is referred to the web version of this article.) Source: [144]. Copyright 2010. Reproduced with permission from the American Chemical Society.

microphase separates into a lamellar structure, and it had previously been shown using GISAXS that, in samples of high molar mass PS-*b*-PB, the lamellae are perpendicular to the substrate, while low molar mass samples orient parallel to the substrate [159]. Papadakis et al. [131] investigated thin films of a low molar mass PS-*b*-PB prepared by spin coating from toluene solution onto Si wafers terminated with an oxide layer. The resulting film was annealed in vacuum at 150 °C for 12 h to remove remaining solvent. Thin films with thicknesses of 210 and 100 nm, respectively, were studied during SVA in toluene, which is a non-selective and good solvent. During SVA, liquid toluene was injected into a reservoir in the sample chamber (Fig. 5a), and the film was thus exposed to a saturated toluene atmosphere (film swelling similar to the one shown in Fig. 5b). During 8 min of SVA, GISAXS maps were recorded every 10 s using an exposure time of 3 s, and the film thickness was measured using a spectroscopic reflectometer.

From the GISAXS maps, it can be seen that the lamellae were parallel to the film during the whole process, and from the position of diffuse Bragg sheets along q_z , the lamellar thickness, D_{lam} , was determined. While the film thickness increased monotonously by more than 50% during uptake of toluene vapor, D_{lam} behaved differently: first, the lamellar thickness increased linearly with time, reaching a maximum of ~15% thickening compared to the bulk value of 18.9 nm, as determined using transmission SAXS.

Then, the lamellar thickness decreased again. In the process, different regimes were identified from the behavior of D_{lam} together with the diffuse Bragg sheet peak intensity and FWHMs along q_z and q_y , respectively. Notably, the diffuse Bragg sheet temporarily extended into an arc in the GISAXS map. It was concluded that the copolymers at first swelled uniaxially (Fig. 17a and b). The blocks then relaxed to a more globular conformation, resulting in an increased interfacial area, and thus a buckling of the lamellar interfaces occurred (Fig. 17c and d). The lamellar stack then broke up and additional lamellae were formed in order to accommodate the increased interfacial area between blocks (Fig. 17d and e). In this regime, the lamellar thickness decreased following $D_{\text{lam}} \propto \phi_p^{0.35}$, which agrees with the prediction made for bulk DBCPs in the strong-segregation limit in a non-selective solvent $D_{\text{lam}} \propto \phi_p^{1/3}$ [113]. Such a restructuring process with formation of additional thinner lamellae seems to be generally occurring in SVA of parallel PS-*b*-PB thin films [111,121], while this process is prohibited in PS-*b*-PB films where the lamellae are perpendicular to the substrate [121,139].

In a later study, a thicker film from a similar PS-*b*-PB DBCP (film thickness 375 nm) was investigated during stepwise swelling with CHX (slightly selective toward PB) using the setup shown in Fig. 5c [111]. The film thickness was increased stepwise (Fig. 5d). The lamellar thickness at the end of each step, i.e. after several minutes of

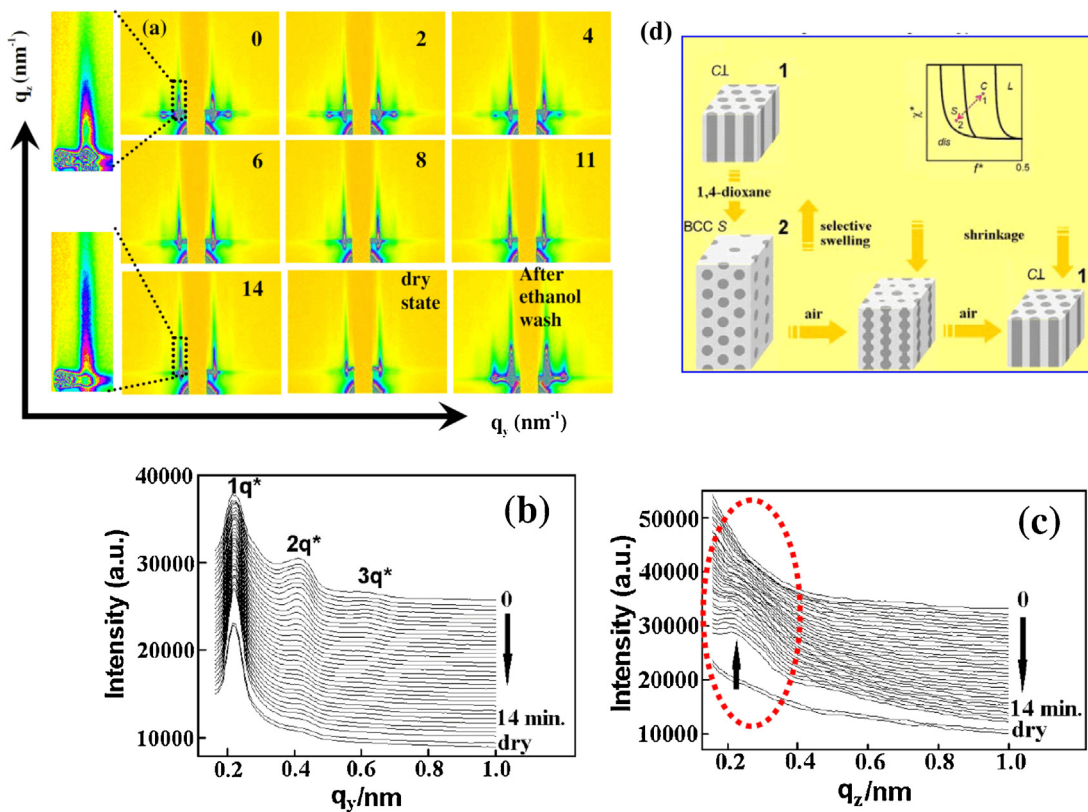


Fig. 16. Results from a PS-*b*-P4VP thin film featuring initially standing cylinders during SVA with 1,4-dioxane. (a) Real-time in situ GISAXS maps during SVA and after drying (second last image) and after ethanol wash (last image). The numbers indicate the SVA time in minutes. In-plane (b) and out-of-plane intensity profiles at $q_y = 0.22 \text{ nm}^{-1}$ (c), both extracted from (a). (d) Schematic representation of the re-orientational process including a schematic phase diagram.

Source: [193]. Copyright 2010. Originally published under a CC BY-NC-SA licence by IOP Publishing.

equilibration, followed the scaling behavior $D_{\text{lam}} \propto \phi_p^{1/6}$, which was predicted for strongly segregated DBCPs in a non-selective solvent, taking the finite width of the lamellar interfaces into account, see Section 2.3.

Zhang et al. investigated thin films of the same low molar mass PS-*b*-PB DBCP during SVA in EAC, which, judging by the value of the Hildebrand solubility parameters, should be a solvent slightly selective for PS, but turned out to act as a non-selective solvent [121]. The as-prepared thin film, which was spun onto an acid-cleaned Si wafer and dried at room temperature in vacuum, featured a mixture of parallel and perpendicular lamellar orientations with the repeat distance (lamellar thickness) depending on orientation. From transmission SAXS on a bulk sample, the repeat distance $D_{\text{lam}}^{\text{bulk}} = 22.0 \pm 0.4 \text{ nm}$ was found. The film was swollen for ~ 45 min letting EAC vapor flow at a rate of $\sim 0.4 \text{ L/h}$ using a sample chamber as shown in Fig. 7a. GISAXS maps were obtained with exposure times varying between 5 and 30 s. Drying was achieved by increasing the flow of inert gas into the cell over a period of ~ 50 min whereupon the EAC flow was turned off and the inert gas flow gradually increased. This protocol allows a high degree of control over the film thickness, as described in Section 3.2.2. Fig. 18 shows the dependence of the repeat distance, D_{lam} , on the polymer volume fraction, ϕ_p , for swelling and

drying. In the as-prepared film, the repeat distance was found from GISAXS to be $14.6 \pm 0.1 \text{ nm}$ for parallel lamellae and $23.0 \pm 0.1 \text{ nm}$ for perpendicular lamellae, the latter of which was close to the value from transmission SAXS, while the parallel repeat distance was 34% smaller. Three regimes were distinguished during swelling: in regime I, the thickness of parallel lamellae, $D_{\text{lam}}^{\text{par}}$, followed a scaling law: $D_{\text{lam}}^{\text{par}} \propto \phi_p^{-\beta}$, with $\beta = 2.2 \pm 0.3$. This is faster than expected from simple volume addition ($\beta = 1$) and was ascribed to inhomogeneous swelling, where the uppermost – parallel – lamellae swell the most. In regime II, the exponent β changed to 5.1 ± 0.3 , i.e. swelling of the parallel lamellae got faster, because the glass transition of the PS block was crossed by taking up solvent, making the chains more mobile.

In contrast to the parallel lamellar distance, the perpendicular lamellar distance stayed much the same during swelling, until the perpendicular lamellae finally disappeared at the end of regime II/beginning of regime III. When $D_{\text{lam}}^{\text{par}}$ had increased to the value found for bulk samples, all orientations followed the same swelling behavior for a while. During swelling, the parallel lamellar stacks broke up and reformed both in regime II and in regime III. All lamellae stayed parallel throughout the rest of the swelling process and during drying; however, $D_{\text{lam}}^{\text{par}}$ decreased in the

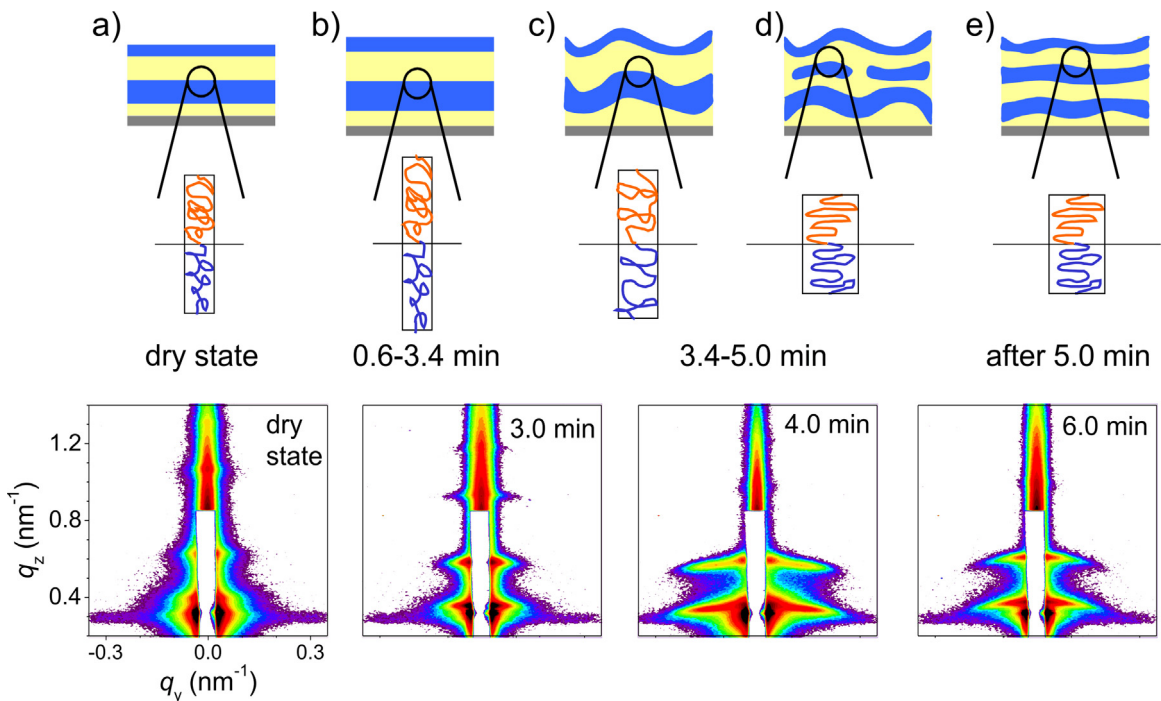


Fig. 17. Top row: Suggested scenario of restructuring of a thin film initially featuring parallel lamellae. Bottom row: Corresponding GISAXS maps. Source: [131], Copyright 2010. Reproduced with permission from the American Chemical Society.

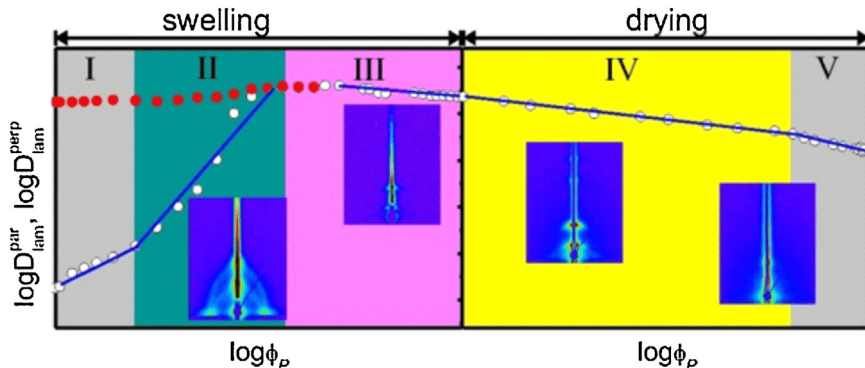


Fig. 18. Results from a low molecular weight PS-*b*-PB thin film during swelling with EAC and subsequent drying. Lamellar thickness of parallel (open circles) and perpendicular lamellae (closed circles) in dependence on ϕ_P , during swelling and drying in a log-log representation. The lines are fits of scaling laws. The corresponding times are given on the top axis. The colors indicate different regimes. Representative 2D GISAXS maps are shown as well. Source: [121], Copyright 2014. Reproduced with permission from the American Chemical Society.

last swelling regime III, where $\beta = -0.32 \pm 0.03$. This corresponds to the previously described mechanism, where additional thinner lamellae were formed to accommodate more coiled chains.

The representative GISAXS maps shown in Fig. 18, illustrate that the lamellar orientation initially was random, i.e. the map featured diffuse Debye–Scherrer ‘rings’. However, due to the orientational dependence of the repeat distance, the rings were distorted. The degree of distortion decreased with increasing $D_{\text{lam}}^{\text{par}}$. In regimes III, IV and V, the GISAXS maps only showed structure along q_z , i.e. all lamellae were parallel. During drying, two regimes were observed: in regime IV, $\beta = -0.43 \pm 0.01$ and in regime V, $\beta = -0.84 \pm 0.04$. The onset of regime V is related to the

PS glass transition temperature which increased above room temperature as solvent left the sample. Finally, a thin film with exclusively parallel lamellae was obtained, with $D_{\text{lam}}^{\text{par}} = 0.91 D_{\text{lam}}^{\text{bulk}}$ being larger than the value in the as-prepared film, $D_{\text{lam}}^{\text{par}} = 0.65 D_{\text{lam}}^{\text{bulk}}$, while the final dry film thickness was the same as for the as-prepared sample. A subsequent study of a similar PS-*b*-PB thin film, where the film was subject to the same SVA cycle twice, revealed that one cycle of SVA is sufficient to bring the film close to equilibrium and to create a nearly defect-free structure [199].

Zhang et al. also studied SVA of high molecular weight compositionally symmetric PS-*b*-PB DCBP films, where the lamellae were perpendicular to the substrate in

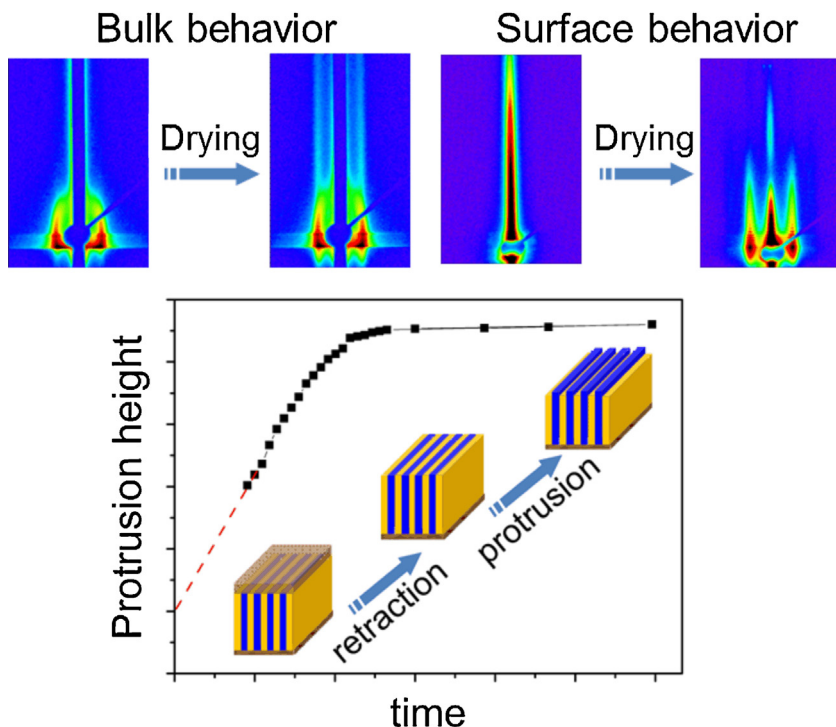


Fig. 19. Results from a high molecular weight PS-*b*-PB thin film during drying. Top: GISAXS maps at high (left) and low (right) incident angle in the fully swollen state and after drying. Bottom: The graph shows the protrusion height as obtained from modeling together with schematic sample structures. Source: [139]. Copyright 2013. Reproduced with permission from John Wiley and Sons.

equilibrium [139]. The thin films were prepared the same way as the sample described in the previous section. SVA was carried out using CHX, a good solvent for PB and a theta solvent for PS. The SVA protocol was similar to the one described in the previous section and GISAXS maps were recorded with 1 min measuring time throughout. For perpendicular lamellae, the restructuring mechanism found in the parallel case and described above, could not take place due to interactions with the substrate and because it would have required unrealistic large-scale mass transport. Instead, the lamellae tilted in order to accommodate more coiling chains and thus thinner lamellae.

By varying the incident angle of the X-ray beam, the near-surface behavior of the film (incident angle below the critical angle of the polymer) can be distinguished from averaging over the full film volume (incident angle above the critical angle of the polymer). It is common procedure to use a rod-shaped beamstop due to intense scattering along q_z for $q_y \sim 0$. However, important structure in the scattered intensity might be obscured by the beamstop, as was found in the following case (Fig. 19). The GISAXS maps shown to the right without the use of a rod-like beamstop revealed scattered intensity from the topmost $\sim 140 \text{ \AA}$, and it was clearly seen that during drying, a modulation in intensity developed along q_z for $q_y \sim 0$.

Model calculations using the lsGISAXS algorithm [157], were consistent with these modulations being due to PS protrusions developing as the solvent left the film and the glass transition temperature for PS shifted to above room

temperature. Fig. 19 shows the protrusion height as function of time. The overall picture was that swelling of the film was one-dimensional along the film normal; i.e. the lateral repeat distance remained unchanged. During swelling, a thin PB layer was formed at the polymer-air interface (PB has a lower surface tension than PS), while the lamellae inside the film were tilting. During drying, the thin PB layer retracted and PS protrusions were formed when the PB selective solvent was leaving the film and the PS domains became glassy, preventing further retraction, while the PB chains continued to be mobile (Fig. 19). In the dry film, the lamellae were perpendicular throughout as evidenced by the occurrence of straight Bragg rods in the GISAXS maps (Fig. 19).

Gu et al. studied thin films of cylinder forming PS-*b*-P2VP during SVA in THF, a near neutral solvent [138,140]. The annealing took place using a sample chamber similar to the one shown in Fig. 5a, and the process was followed *in situ* with GISAXS using 20 s exposure time. The samples were prepared by spin coating onto silicon wafers having a native oxide layer and cleaned using oxygen plasma. The as-prepared film featured lying cylinders. It was found that both solvent removal rate and swelling rate played important roles for the repeat distance and the extent of lateral order in the dry structure. Specifically, it was found that a relatively fast solvent removal rate was required to freeze in the ordered structure of a swollen film [138]. The authors simulated 2D GISAXS maps using HipGISAXS [187] and were thus able to distinguish films constructed from 4, 5 and 6 layers of lying cylinders by comparing

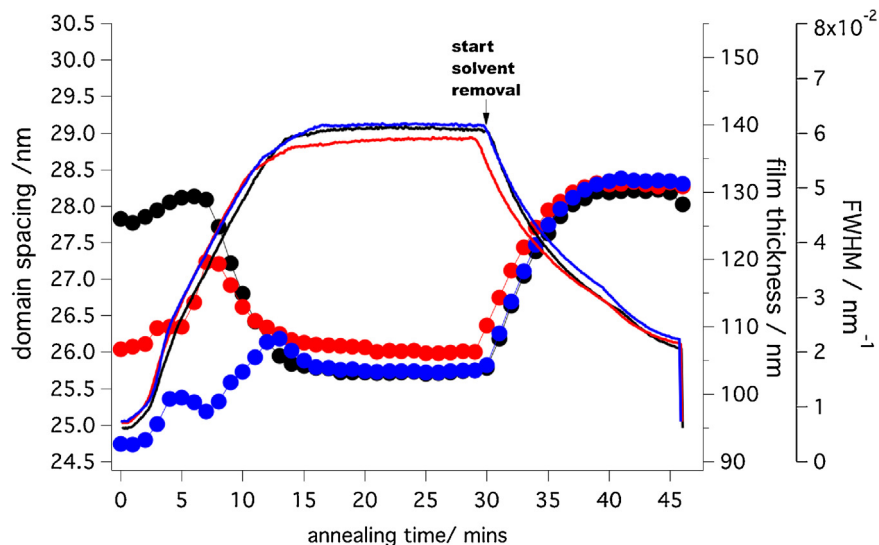


Fig. 20. Results of in situ GISAXS experiments during SVA of PS-*b*-P2VP in THF and during drying. Film thickness (full lines) and domain spacings (circles) of three different samples (denoted by different colors) in dependence of annealing time. The three samples had been processed in different ways and have therefore different initial domain spacings. (For interpretation of the references to colour in this figure legend, the reader is referred to the web version of this article.)

Source: [140]. Copyright 2014. Reproduced with permission from Springer.

the finer details in the intensity of a Bragg reflection with experimental results. Results from three similar films with different processing histories showed that differences in structure resulting from the differences in processing were erased when the samples were swollen by more than 40%. In Fig. 20, data for repeat distance and film thickness during SVA are shown [140]. Each sample had a different starting morphology depending on processing (spin coated with no further processing, spin coated followed by SVA, and instantaneous removal of solvent, and spin coated followed by SVA with slow removal of solvent). However, after a swelling ratio of 1.4 was reached, where the chains had obtained a certain mobility and unfavorable interactions were screened sufficiently, the samples followed the same structural evolution.

These results clearly highlight the potential of using in situ, real-time GISAXS, especially in combination with the rapidly developing software for analysis and simulation of 2D GISAXS maps, to obtain very detailed information about the morphological changes during the SVA process – as the film swells, equilibrates, deswells, and goes through thickness and morphology changes – and about the underlying mechanisms. This knowledge is of fundamental importance to understand the pathways leading to the final film morphology after drying and thus being able to obtain control over the process. Such knowledge is also an essential requirement for a future industrial production of nanostructured coatings of consistent quality.

5. Future application areas for in situ studies

In recent years, the interest in SVA has grown considerably, partly motivated by technological developments, e.g. in nanotechnological engineering using DSA in the semiconductor industry, and research and development for

the next generation of data storage technology. DSA typically involves a SVA step, in order to reach the required degree of perfection of the manufactured structures. The BCP is used as a template for successive processing steps, such as reactive ion etching. Moreover, the development of high-density magnetic storage media, where the block copolymer structure is used to position a layer of magnetic nanoparticles at well determined locations, has sparked the interest in SVA of BCP thin films. A few issues, such as the possibility of an increased roughness or even dewetting, which have been encountered in certain cases upon prolonged swelling and fast drying [195], as well as the use of carcinogenic solvents to obtain specific structures, have to be resolved, especially for large-scale applications in industrial environments.

In the remainder of this review, we address current developments which may initiate new research directions in the field of in situ investigations of BCP thin films during SVA. Notably, novel scattering techniques are being implemented, new systems for SVA are being developed, and SVA is used as a component in new structure preparation techniques. In situ real-time GISAXS is a unique technique to reveal self-organization pathways and to improve our understanding of the underlying polymer physics.

5.1. Enhancement of scattering contrast

An important issue in GISAXS experiments during SVA is the variation of X-ray contrast, i.e. the electron density differences between various regions in the sample and the variation of this contrast during solvent vapor uptake which will influence the scattering intensity. Solvent selectivity and the inhomogeneous distribution of solvent in the BCP thin film during swelling and drying are important

related issues. For instance, the theoretically predicted solvent concentration gradient throughout the sample during drying in dependence on the evaporation rate needs to be quantified and further characterized [96,97,99], along with related issues such as a possible accumulation of solvent at the interfaces of the BCP morphology, the influence of the solvent on the glass transition [204] and the possible initiation of microphase separation at the film/substrate interface [205]. Another important aspect, as previously discussed, is that the different swelling behavior of the microdomains in dependence on the solvent selectivity – which may be concentration-dependent – in certain cases may lead to morphological transitions as well as to changes in contrast [133,144,193,194].

The need for high scattering contrast between microdomains becomes even more important for multi-block copolymers, for use of solvent mixtures for SVA or when functional molecules or nanoparticles are incorporated in the BCP thin films. Usually, GISAXS is carried out at X-ray energies of 8–10 keV, and scattering contrast is due to electron density differences in the BCP thin film. Anomalous GISAXS with soft (below 1 keV) or tender (2–5 keV) X-rays allows highlighting certain components as well as contrast matching by varying the X-ray wavelength around the absorption edges of the BCPs. This is especially interesting for multicomponent systems, such as triblock copolymer thin films, as demonstrated by Wang et al. studying PI-*b*-PS-*b*-P2VP triblock copolymers [206]. In this work, resonant soft X-ray scattering in transmission geometry was carried out at X-ray energies of 250–284 eV to discriminate between different blocks using the pronounced resonances of different carbon bonds around the carbon K-edge. This study was combined with SAXS and GISAXS using standard conditions (10 keV). Grazing-incidence soft X-ray scattering (GISoXS), i.e. the combination of both techniques, is currently emerging [227,228].

Using neutrons as a probe instead of X-rays, contrast between different components may be enhanced by (partially) deuterating certain blocks of the BCP thin film or the solvent (GISANS [207]). As an alternative to monochromatic GISANS, time-of-flight GISANS has been developed, covering a wide range of momentum transfers in a single measurement [208], which compensates partly for the much lower neutron flux compared to the X-ray flux at synchrotron sources. So far, BCP thin films have only been investigated in the dry state with time-of-flight GISANS [209,210]. Due to the wide range of incident wave lengths covered, near-surface and bulk structures are detected in a single measurement, differently from monochromatic experiments where the incident angle has to be varied to achieve this depth sensitivity. In both cases, however, the measurement time is still too long (typically several hours), and time-resolved GISANS measurements with a time resolution of a few seconds thus remain a challenge. However, quasi-static in situ experiments on films with well-controlled swelling using deuterated solvents for contrast are conceivable and a valuable supplement to GISAXS, where good solvent contrast is difficult to obtain.

5.2. New approaches to SVA

The time needed for SVA of BCP thin films with the aim of obtaining a certain structural change, is often too long for the demands of the semiconductor industry. One reason is the high partial pressure of air when working at ambient conditions which can result in slow film swelling because, under these conditions, the solvent vapor build-up is diffusion-limited. Long tubes may also hamper fast changes of conditions. Chambers with a very small volume and evacuation of the sample chamber before injection of liquid solvent [40,211] have been proposed. This way, the time needed for SVA may be reduced from several hours to several minutes.

For *in situ* GISAXS experiments, these short timescales open up the possibility of doing many more annealing cycles during a given synchrotron beamtime to test reversibility and aging. Moreover, in a vacuum environment, the polymer swelling kinetics can be distinguished from the slow vapor pressure build-up (minutes) in a standard ambient SVA cell. Other approaches include SVA at elevated temperatures [146,198] and the use of a solvent-trapping layer underneath the block copolymer thin film during thermal annealing [212].

Spectacular results have been obtained using *directional* solvent vapor flow in SVA of PS-*b*-PEO thin films [174]. Highly ordered nanostructures with lying, crystalline PEO cylinders within a PS matrix were achieved. The cylinders were well ordered in domains of several micrometers due to shearing effects of the flow of benzene vapor parallel to the surface.

SVA of BCP thin films has so far mostly been carried out with single solvents having a certain quality and selectivity for the different blocks of the BCP (see Section 4). SVA requires solvents which have a vapor pressure in a certain range and, moreover, safety concerns may put limitations to the choice of solvents. Such boundary conditions can hamper the exploration of the full parameter space and the fine tuning and optimization of conditions. Combining a non-selective with a selective solvent or two solvents being selective for either block and varying the mixing ratio may overcome these limitations and pave the way for a systematic variation of the degree of swelling of the different microdomains. Very detailed studies of the influence of the properties of solvent mixtures on the thin film structures have been reported; however, so far mostly *ex situ* investigations have been carried out [92,211,213–219].

Chavis et al. [218] reported a real-time *in situ* SVA on a symmetric PHEMA-*b*-PMMA DBCP using a methanol and THF mixture (THF and methanol are selective for PMMA and for PHEMA, respectively). Depending on the mixing ratio, different morphologies could be obtained apart from the equilibrium parallel lamellar structure: lying cylinders, BCC spheres, and the gyroid structure. These phases obtained at high swelling ratios could be quenched by rapid drying, albeit with a deformation of the domains due to the pronounced vertical shrinkage of the films during drying. An unusual kinetic pathway was revealed: the gyroid phase only appeared during drying after a long vapor anneal of 5 h in a 50:50 mixture; using a shorter annealing time,

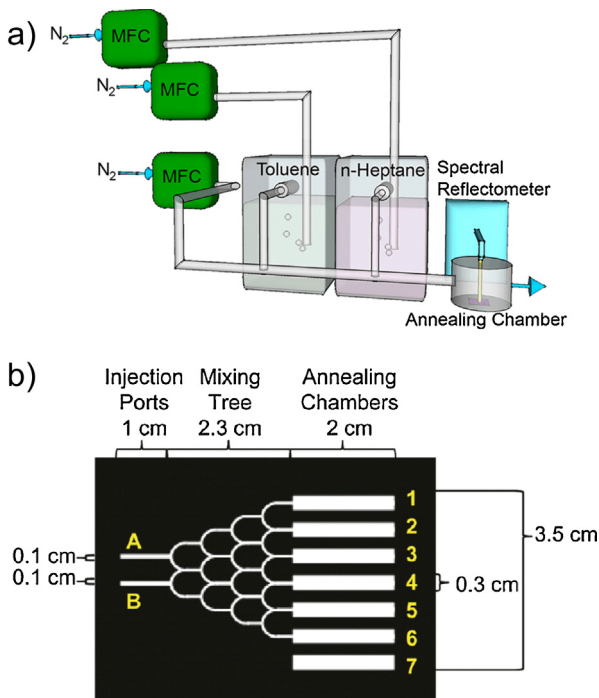


Fig. 21. Devices for SVA with solvent mixtures. (a) Device for SVA with two saturated solvents including two bubblers and a chamber featuring a film thickness monitor. (b) Device design for gradient SVA. Solvent vapors enter through injection ports A and B, mix in the mixing tree, and pass through annealing chambers 1–6. Chamber 7 is detached from the mixing tree and serves as a control chamber.

Source: (a) [92]. Copyright 2012. Reproduced with permission from the American Chemical Society. (b) [214]. Copyright 2011. Reproduced with permission from the American Chemical Society.

metastable BCC spheres were kinetically trapped in the dry state.

Gotrik et al. implemented a chamber for simultaneous SVA of thin films of PS-*b*-PDMS DBCPs with vapors from two selective solvents, toluene and *n*-heptane, together with an inert gas (Fig. 21a) and demonstrated that a variety of morphologies can be created in thin films of PS-*b*-PDMS DBCPs [92], depending on the relative flow rates of the two solvents. This system was recently used for in situ real-time GISAXS experiments [195]: thin films from PS-*b*-PDMS diblock copolymers were investigated in situ using the vapor of a mixture of toluene/heptane 5:1 v/v which is close to non-selective for PS and PDMS. A reorientation from standing to lying cylinders during swelling which was preserved during drying and which was attributed to preferential surface interactions. Drying led to a strong reduction of the lattice spacing along the film normal, but only a very weak one in the film plane, with the distortion ratio depending on the drying rate. The dependence of the time needed for achieving a well-defined cylindrical structure was found to increase with the initial film thickness, which the authors tentatively attributed to a solvent concentration gradient in thick films.

Cetintas and Kamperman [220] carried out SVA of PS-*b*-PNIPAM-*b*-PS thin films using a mixture of methanol

(selective for PNIPAM) and THF (almost non-selective) 1:2 v/v and found, using in situ GISAXS, that the original lamellar structure was transformed into hexagonally ordered, standing PS cylinders in a PNIPAM. In contrast, a mixture of methanol and toluene (selective for PS) 1:1 v/v resulted in the inverse morphology, namely standing PNIPAM cylinders in a PS matrix. No long-range order could be obtained when only one type of solvent was used. The authors pointed out that the difference of vapor pressures may play a role for the uptake of the respective solvent in the film.

A microfluidic mixing device developed by Albert et al. (Fig. 21b) offers precise control over the mixing ratio of the two solvents for each of the outlets [214]. AFM revealed structural differences between samples in the different annealing chambers, all obtained in a single SVA experiment, thus reducing random artifacts. This approach also lends itself to combinatorial studies where a large range of solvents and vapor concentrations is probed.

Raster solvent annealing is another promising development: a vapor nozzle is moved over the BCP thin film allowing spatially resolved SVA and thus to control the structure of the BCP thin film locally. By varying the rastering speed [216], different kinetic regimes can be probed. Moreover, raster annealing is compatible with roll-to-roll processing of larger polymer quantities. To the best of our knowledge, these refined methods for SVA have not been used in combination with in situ GISAXS. Especially interesting in this context may be GISAXS using X-ray microbeams [221,222].

5.3. Macroscopic orientation by combining SVA with other methods

While SVA has been shown to improve the degree of long-range order of the BCP thin film structures substantially (Section 4.1), this is often not sufficient or reliable enough for applications requiring perfect order, such as nanolithography or magnetic data storage. Park et al. [223] reported the self-assembly of PS-*b*-PEO guided by a sapphire substrate with a sawtooth topography. After SVA in benzene and water vapor, perfectly ordered arrays of standing cylinders in microdomains with an area of ~4 cm² were obtained. The 3 nm diameter cylinders with a center-to-center distance of 6.9 nm produced area densities in excess of 10 Terabit per square inch. Using GISAXS and rotating the film about the surface normal, discrete directions of a two-dimensional hexagonal array were found (Fig. 22). Based on the GISAXS results, the authors concluded that the film consisted of a single hexagonal array and that the in-plane ordering was perfect over the entire surface.

The demonstration of DSA [42–44,224,225], in which a micropatterned or nanopatterned substrate directs the orientation of the BCP domains, has caught the attention of the semiconductor industry. Current photolithographical methods are close to a 14 nm feature size. In this situation, a hybrid approach appears attractive: if polymer photoresists can be found that form appropriate structures such as lying cylinders or standing lamellae

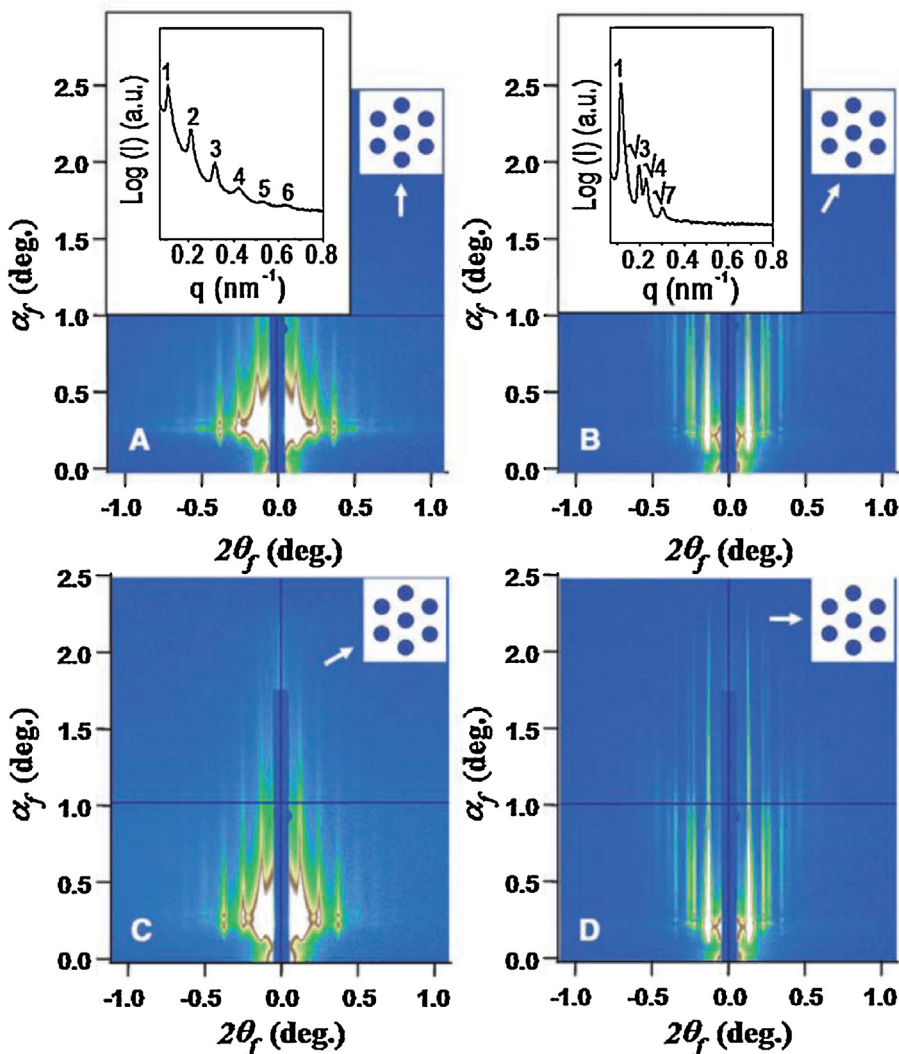


Fig. 22. GISAXS patterns of PS-*b*-PEO thin films annealed in benzene and water vapors. The insets show the schematic 2D hexagonal lattices with the incoming beam direction marked by an arrow. When the sample stage was rotated by 0° or 60°, the GISAXS patterns show integer-order diffraction peaks (A and C). When the sample stage was rotated by 30° or 90°, diffraction peaks from the (11) and (21) lattice lines are seen (B and D). Line profiles of the scattering as a function of the in-plane scattering vector, q , are shown in the insets at the left in (A) and (B). Source: [223]. Copyright 2009. Reproduced with permission from the American Association for the Advancement of Science.

in lithographic grooves, feature sizes below 10 nm may be reached [44]. Other applications, e.g. in photonics, require larger repeat distances and thus the use of high molar mass DBCP thin films. Since long-range order is difficult to achieve due to low chain mobility and a large number of entanglements, SVA with a non-selective solvent combined with thermal annealing and a topographically patterned substrate offers a way to prepare highly ordered films [92,133,213,225,226]. Alternatively, chemically patterned substrates can be used [45]. Common to all DSA approaches is a SVA step that improves the lateral order of the DBCP morphologies on the structured templates. A number of studies have been carried out and show impressive results; however, they build on ex situ characterization.

6. Conclusion

SVA offers the possibility to obtain a large degree of control over the structures of BCP thin films. In situ GISAXS has emerged as the ultimate technique to provide real-time characterization of the SVA process and the BCP morphology. Such studies can provide much more detailed information on the structural changes during SVA of BCP thin films than classical ex situ studies, where imaging methods or ex situ GISAXS are used before and after SVA. A variety of sample environments has been developed for in situ GISAXS studies during SVA which allow covering a large range of conditions, e.g. working at different vapor pressures or swelling and drying rates. A number of spectacular in situ studies have elucidated the

pathways of restructuring under different annealing conditions. SVA has been used to improve the degree of order in the films, to control the orientation of the microdomains as well as to change the morphology. A number of parameters are of importance for the SVA process: the initial state of the BCP thin film, the choice of solvent, the maximum degree of swelling and the rate of drying. Whereas in many studies, single GISAXS measurements were carried out at certain degrees of swelling, few studies have addressed the pathways of structural reorganization by exploiting the time-resolution at synchrotron beamlines. These latter studies have revealed mechanisms of restructuring which can be compared with the results from theory and computer simulations and help to gain a deeper understanding of the SVA process.

Theoretical simulations on supercomputers are emerging to model the reorganization processes in BCP thin films; however, only few studies have been carried out so far, pointing to the importance of an inhomogeneous solvent distribution in the film, the change of the glass transition temperature by the solvent, and the rate of solvent removal compared to the relaxation rate of the BCPs, among other issues. These results will provide fertile grounds for future *in situ* experiments. Combination of experiment and simulation are expected to establish a set of general rules, how to best anneal a given BCP thin film to obtain a specific well-ordered structure.

The examples given in this review show that the field is in rapid development; both with respect to understanding the mechanisms of restructuring in BCP thin films during SVA as well as reaching the application stage on a large scale, especially in combination with other structure-directing methods. *In situ* real-time GISAXS – carried out at synchrotron beamlines – is of key importance to drive this development.

Acknowledgements

We thank (in alphabetical order) P. Busch, Z. Di, R. Li, J. Perlich, M. Rauscher, S.V. Roth, and A. Sepe for good collaboration. Deutsche Forschungsgemeinschaft, the Russian Foundation for Basic Research, the North Atlantic Treaty Organization (NATO), the Graduate School of Excellence ‘Complex Materials at Interfaces’ and DANSCATT (Danish Instrument Centre for the Use of Synchrotron X-ray and Neutron Facilities) are thanked for financial support. The Cornell High Energy Synchrotron Source (CHESS) is supported by the National Science Foundation (NSF) and the National Institutes of Health and General Medical Sciences (NIH/NIGMS) via NSF award DMR-1332208. We thank (in alphabetical order) CHESS and Deutsches Elektronen-Synchrotron (DESY) for beamtime and excellent equipment.

References

- [1] Ramanathan M, Darling SB. Mesoscale morphologies in polymer thin films. *Prog Polym Sci* 2011;36:793–811.
- [2] Xue L, Zhang J, Han Y. Phase separation induced ordered patterns in thin polymer blend films. *Prog Polym Sci* 2012;37:564–94.
- [3] Park M, Harrison C, Chaikin PM, Register RA, Adamson DH. Block copolymer lithography: periodic arrays of 10^{11} holes in 1 square centimeter. *Science* 1997;276:1401–4.
- [4] Stoykovich MP, Kang H, Daoulas KC, Liu G, Liu CC, de Pablo JJ, et al. Directed self-assembly of block copolymers for nanolithography: fabrication of isolated features and essential integrated circuit geometries. *ACS Nano* 2007;1:168–76.
- [5] Park S, Kim B, Wang JY, Russell TP. Fabrication of highly ordered silicon oxide dots and stripes from block copolymer thin films. *Adv Mater* 2008;20:681–5.
- [6] Bang J, Jeong U, Ryu DY, Russell TP, Hawker CJ. Block copolymer nanolithography: translation of molecular level control to nanoscale patterns. *Adv Mater* 2009;21:4769–92.
- [7] Chang SW, Chuang VP, Boles ST, Ross CA, Thompson CV. Densely packed arrays of ultra-high-aspect-ratio silicon nanowires fabricated using block-copolymer lithography and metal-assisted etching. *Adv Funct Mater* 2009;19:2495–500.
- [8] Cheng JY, Sanders DP, Truong HD, Harrer S, Friz A, Holmes S, et al. Simple and versatile method to integrate directed self-assembly with optical lithography using a polarity-switched photoresist. *ACS Nano* 2010;4:4815–23.
- [9] Tsai HY, Miyazoe H, Engelmann S, To B, Sidorski E, Buccignano J, et al. Sub-30 nm pitch line-space patterning of semiconductor and dielectric materials using directed self-assembly. *J Vac Sci Technol B* 2012;30, 06FB205/1–6.
- [10] Brendel JC, Liu F, Lang AS, Russell TP, Thelakkat M. Macroscopic vertical alignment of nanodomains in thin films of semiconductor amphiphilic block copolymers. *ACS Nano* 2013;7:6069–78.
- [11] Jeong JW, Hur YH, Kim HJ, Kim JM, Park WI, Kim MJ, et al. Proximity injection of plasticizing molecules to self-assembling polymers for large-area, ultrafast nanopatterning in the sub-10-nm regime. *ACS Nano* 2013;7:6747–57.
- [12] Kang Y, Walsh JJ, Gorishnyy T, Thomas EL. Broad-wavelength-range chemically tunable block-copolymer photonic gels. *Nat Mater* 2007;6:957–60.
- [13] Jung YS, Jung W, Tuller HL, Ross CA. Nanowire conductive polymer gas sensor patterned using self-assembled block copolymer lithography. *Nano Lett* 2008;8:2776–80.
- [14] Mistark PA, Park S, Yalcin SE, Lee DH, Yavuzcetin O, Tuominen MT, et al. Block-copolymer-based plasmonic nanostructures. *ACS Nano* 2009;3:3987–92.
- [15] Thurn-Albrecht T, Schotter J, Kästle GA, Emley N, Shibauchi T, Krusin-Elbaum L, et al. Ultrahigh-density nanowire arrays grown in self-assembled diblock copolymer templates. *Science* 2000;290:2126–9.
- [16] Du P, Li M, Douki K, Li X, Garcia CBW, Jain A, et al. Additive-driven phase-selective chemistry in block copolymer thin films: the convergence of top-down and bottom-up approaches. *Adv Mater* 2004;16:953–7.
- [17] Tokarev I, Krenek R, Burkov Y, Schmeisser D, Sidorenko A, Minko S, et al. Microphase separation in thin films of poly(styrene-block-4-vinylpyridine) copolymer-2-(4'-hydroxybenzeneazo)benzoic acid assembly. *Macromolecules* 2005;38:507–16.
- [18] Son JG, Bae WK, Kang H, Nealey PF, Char K. Placement control of nanomaterial arrays on the surface-reconstructed block copolymer thin films. *ACS Nano* 2009;3:3927–34.
- [19] Chao CC, Wang TC, Ho RM, Georgopoulos P, Avgeropoulos A, Thomas EL. Robust block copolymer mask for nanopatterning polymer films. *ACS Nano* 2010;4:2088–94.
- [20] Chinthamanipta PS, Lou Q, Shipp DA. Periodic titania nanostructures using block copolymer templates. *ACS Nano* 2011;5:450–6.
- [21] Wu NLY, Zhang X, Murphy JN, Chai J, Harris KD, Buriak JM. Density doubling of block copolymer templated features. *Nano Lett* 2012;12:264–8.
- [22] Liu Z, Huang H, He T. Large-area 2D gold nanorod arrays assembled on block copolymer templates. *Small* 2013;9:505–10.
- [23] Lee JG, Jung YS, Han SH, Kim KM, Han YK. Long-range ordered self-assemblies of novel acrylamide-based diblock copolymers for nanolithography and metallic nanostructure fabrication. *Adv Mater* 2014;26:2894–900.
- [24] Cui G, Fujikawa M, Nagano S, Sano M, Takase H, Miyazaki T, et al. Perpendicular oriented cylinders via directional coalescence of spheres embedded in block copolymer films induced by solvent annealing. *Polymer* 2014;55:1601–8.
- [25] Dinda S, Suresh V, Das D, Gupta RK. Gold nanoparticles adsorption onto periodic block copolymer using quartz crystal microbalance. *Mater Lett* 2015;148:118–21.

- [26] Li M, Douki K, Goto K, Li X, Coenjarts C, Smilgies DM, et al. Spatially controlled fabrication of nanoporous block copolymers. *Chem Mater* 2004;16:3800–8.
- [27] Nagarajan S, Li M, Pai RA, Bosworth JK, Busch P, Smilgies DM, et al. An efficient route to mesoporous silica films with perpendicularly nanochannels. *Adv Mater* 2008;20:246–51.
- [28] Crossland E, Kamperman M, Nedelcu M, Ducati C, Wiesner U, Toombes G, et al. A bicontinuous double gyroid hybrid solar cell. *Nano Lett* 2009;9:2807–12.
- [29] Lee DH, Park S, Gu W, Russell TP. Highly ordered nanoporous template from triblock copolymer. *ACS Nano* 2011;5:1207–14.
- [30] Zhang R, Dutriez C, Sugiyama K, Ishizone T, Yokoyama H. Thermally robust nanocellular thin films of high- T_g semifluorinated block copolymers foamed with supercritical carbon dioxide. *Soft Matter* 2011;7:4032–8.
- [31] Marques DS, Dorin RM, Wiesner U, Smilgies DM, Behzad AR, Vainio U, et al. Time-resolved grazing-incidence small-angle scattering and cryomicroscopy characterization of block copolymer membrane formation. *Polymer* 2014;55:1327–32.
- [32] Zhang Y, Sargent JL, Boudouris BW, Phillip WA. Nanoporous membranes generated from self-assembled block polymer precursors: Quo vadis? *J Appl Polym Sci* 2015;132, 41683/1–17.
- [33] Fasolka MJ, Mayes AM. Block copolymer thin films: physics and applications. *Annu Rev Mater Res* 2001;31:323–55.
- [34] Lazzari M, López-Quintela MA. Block copolymers as a tool for nano-material fabrication. *Adv Mater* 2003;15:1583–94.
- [35] Segalman RA. Patterning with block copolymer thin films. *Mater Sci Eng Rep* 2005;48:191–226.
- [36] Hamley IW. Ordering in thin films of block copolymers: fundamentals to potential applications. *Prog Polym Sci* 2009;34:1161–210.
- [37] Kim HC, Park SM, Hinsberg WD. Block copolymer based nanostructures: materials, processes, and applications to electronics. *Chem Rev* 2010;110:146–77.
- [38] Knoll A, Magerle R, Krausch G. Phase behavior in thin films of cylinder-forming ABA block copolymers: experiments. *J Chem Phys* 2004;120:1105–16.
- [39] Elbs H, Krausch G. Ellipsometric determination of Flory–Huggins interaction parameters in solution. *Polymer* 2004;45:7935–42.
- [40] Gong Y, Li Y, He Y, Wang L, Huang H, He T. Solvent-vapor-induced rapid assembly of block-copolymer film via prevacuumizing. *Macromol Chem Phys* 2014;215:1092–7.
- [41] Kim SO, Solak HH, Stoykovich MP, Ferrier NJ, de Pablo JJ, Nealey PF. Epitaxial self-assembly of block copolymers on lithographically defined nanopatterned substrates. *Nature* 2003;424:411–4.
- [42] Cheng JY, Mayes AM, Ross CA. Nanostructure engineering by templated self-assembly of block copolymers. *Nat Mater* 2004;3:823–8.
- [43] Bosworth JK, Paik MY, Ruiz R, Schwartz EL, Huang JQ, Ko AW, et al. Control of self-assembly of lithographically patternable block copolymer films. *ACS Nano* 2008;2:1396–402.
- [44] Kennemur JG, Yao L, Bates FS, Hillmyer MA. Sub 5 nm domains in ordered poly(cyclohexylethylene)-block-poly(methyl methacrylate) block polymers for lithography. *Macromolecules* 2014;47:1411–8.
- [45] Li S, Wan L, Liu CC, Nealey PF. Directed self-assembly of block copolymers on chemical patterns: a platform for nanofabrication. *Prog Polym Sci* 2016;54:76–127.
- [46] Sinturel C, Vayer M, Morris M, Hillmyer MA. Solvent vapor annealing of block polymer thin films. *Macromolecules* 2013;46:5399–415.
- [47] Shelton CK, Epps III TH. Block copolymer thin films: characterizing nanostructure evolution with in situ X-ray and neutron scattering. *Polymer* 2016, <http://dx.doi.org/10.1016/j.polymer.2016.06.069>.
- [48] Majewski PW, Yager KG. Rapid ordering of block copolymer thin films. *J Phys: Condens Matter* 2016;28, 403002/1–37.
- [49] Naudon A. Grazing-incidence small-angle X-ray scattering application to layers and surface layers. In: Brumberger H, editor. Modern aspects of small-angle scattering. Amsterdam: Kluwer Academic Publishers; 1995. p. 181–202.
- [50] Müller-Buschbaum P. Grazing incidence small-angle X-ray scattering – an advanced scattering technique for the investigation of nanostructured polymer films. *Anal Bioanal Chem* 2003;376:3–10.
- [51] Müller-Buschbaum P. A basic introduction to grazing incidence small-angle X-ray scattering. *Lect Notes Phys* 2009;776:61–89.
- [52] Renaud G, Lazzari R, Leroy F. Probing surface and interface morphology with grazing incidence small angle X-ray scattering. *Surf Sci Rep* 2009;64:255–380.
- [53] Ree M. Probing the self-assembled nanostructures of functional polymers with synchrotron grazing incidence X-ray scattering. *Macromol Rapid Commun* 2014;35:930–59.
- [54] Hexemer A, Müller-Buschbaum P. Advanced grazing-incidence techniques for modern soft matter materials analysis. *IUCrJ* 2015;2:106–25.
- [55] Müller-Buschbaum P. GISAXS and GISANS as metrology technique for understanding the 3D morphology of block copolymer thin films. *Eur Polym J* 2016;81:470–93.
- [56] Shull KR. Mean-field theory of block copolymers: bulk melts, surfaces, and thin films. *Macromolecules* 1992;25:2122–33.
- [57] Turner MS. Equilibrium properties of a diblock copolymer lamellar phase confined between flat plates. *Phys Rev Lett* 1992;69:1788–91.
- [58] Pickett GT, Witten TA, Nagel SR. Equilibrium surface orientation of lamellae. *Macromolecules* 1993;26:3194–9.
- [59] Kikuchi M, Binder KJ. Microphase separation in thin films of the symmetric diblock-copolymer melt. *Chem Phys* 1994;101:3367–77.
- [60] Walton DG, Kellogg GJ, Mayes AM, Lambooy P, Russell TP. A free energy model for confined diblock copolymers. *Macromolecules* 1994;27:6225–8.
- [61] Geisinger T, Müller M, Binder K. Symmetric diblock copolymers in thin films. I. Phase stability in self-consistent field calculations and Monte Carlo simulations. *J Chem Phys* 1999;111:5241–50.
- [62] Huinink HP, Brokken-Zijp JCM, van Dijk MA, Sevink GJA. Asymmetric block copolymers confined in a thin film. *J Chem Phys* 2000;112:2452–62.
- [63] Huinink HP, van Dijk MA, Brokken-Zijp JCM, Sevink GJA. Surface-induced transitions in thin films of asymmetric diblock copolymers. *Macromolecules* 2001;34:5325–30.
- [64] Wang Q, Nealey PF, de Pablo JJ. Monte Carlo simulations of asymmetric diblock copolymer thin films confined between two homogeneous surfaces. *Macromolecules* 2001;34:3458–70.
- [65] Knoll A, Horvat A, Lyakhova KS, Krausch G, Sevink GJA, Zvelindovsky AV, et al. Phase behavior in thin films of cylinder-forming block copolymer. *Phys Rev Lett* 2002;89, 035501/1–4.
- [66] Szamel G, Müller M. Thin films of asymmetric triblock copolymers: a Monte Carlo study. *J Chem Phys* 2003;118:905–13.
- [67] Horvat A, Lyakhova KS, Sevink GJA, Zvelindovsky AV, Magerle R. Phase behavior in thin films of cylinder-forming ABA block copolymers: mesoscale modelling. *J Chem Phys* 2004;120:1117–26.
- [68] Pereira GG. Cubic to cylindrical transition in diblock copolymers induced by strain. *Macromolecules* 2004;37:1611–20.
- [69] Potemkin II, Möller M. Microphase separation in ultrathin films of diblock copolymers with variable stickiness of one of the blocks to the surface. *Macromolecules* 2005;38:2999–3006.
- [70] Yang Y, Qiu F, Zhang H, Yang Y. Cylindrical phase of diblock copolymers confined in thin films. A real-space self-consistent field theory study. *Polymer* 2006;47:2205–16.
- [71] Yin Y, Sun P, Jiang R, Li B, Chen T, Jin Q, et al. Simulated annealing study of asymmetric diblock copolymer thin films. *J Chem Phys* 2006;124, 184708/1–8.
- [72] Chen P, Liang HJ, Shi AC. Origin of microstructures from confined asymmetric diblock copolymers. *Macromolecules* 2007;40:7329–35.
- [73] Stein GE, Cochran EW, Katsov K, Fredrickson GH, Kramer EJ, Li X, et al. Symmetry breaking of in-plane order in confined copolymer mesophases. *Phys Rev Lett* 2007;98:158302.
- [74] Patyukova ES, Potemkin II. Nanostructured ultrathin films obtained by the spreading of diblock copolymers on a surface. *Langmuir* 2007;23:12356–65.
- [75] Heckmann M, Drossel B. Cylindrical phase of block copolymers in thin films. *Macromolecules* 2008;41:7679–86.
- [76] Sevink GJA, Zvelindovsky AV. Confined sphere-forming block copolymers: phase behavior and the role of chain architecture. *Macromolecules* 2009;42:8500–12.
- [77] Tan H, Song Q, Niu X, Wang Z, Gao W, Yan D. Sphere-forming diblock copolymers in slit confinement: a dynamic density functional theory study. *J Chem Phys* 2009;130, 214901/1–7.
- [78] Yu B, Li B, Jin Q, Ding D, Shi AC. Confined self-assembly of cylinder-forming diblock copolymers: effects of confining geometries. *Soft Matter* 2011;7:10227–40.
- [79] Li W, Liu M, Qiu F, Shi AC. Phase diagram of diblock copolymers confined in thin films. *J Phys Chem B* 2013;117:5280–8.
- [80] Hannon AF, Bai W, Alexander-Katz, Ross CA. Simulation methods for solvent vapor annealing of block copolymer thin films. *Soft Matter* 2015;11:3794–805.

- [81] Matsen MW. Thin films of block copolymer. *J Chem Phys* 1997;106:7781–91.
- [82] Wang Q, Yan Q, Nealey PF, de Pablo JJ. Monte Carlo simulations of diblock copolymer thin films confined between two homogeneous surfaces. *J Chem Phys* 2000;112:450–64.
- [83] Meng D, Wang Q. Complex morphologies in thin films of symmetric diblock copolymers as stable and unstable phases. *Soft Matter* 2010;6:5891–906.
- [84] Bai W, Hannon AF, Gotrik KW, Choi HK, Aissou K, Lontos G, et al. Thin film morphologies of bulk-gyroid polystyrene-block-polydimethylsiloxane under solvent vapor annealing. *Macromolecules* 2014;47:6000–8.
- [85] Sun YS, Chien SW, Liou JY. Probing relief terraces in destabilized thin films of an asymmetric block copolymer with grazing-incidence small-angle X-ray scattering. *Macromolecules* 2010;43:7250–60.
- [86] Guo ZY, Lin MS, Chang YT, Sun YS, Chiang YW, Chou CY, et al. Surface relief terraces and self-assembled nanostructures in thin block copolymer films with solvent annealing. *Polymer* 2012;53:4827–33.
- [87] Potemkin II. Lamellar orientation in thin, supported diblock copolymer films: strong segregation theory. *Macromolecules* 2004;37:3505–9.
- [88] Potemkin II, Busch P, Smilgies DM, Posselt D, Papadakis CM. Effect of the molecular weight of AB diblock copolymers on the lamellar orientation in thin films: theory and experiment. *Macromol Rapid Commun* 2007;28:579–84.
- [89] Stasiak P, McGraw JD, Dalmoki-Veress K, Matsen MW. Step edges in thin films of lamellar-forming diblock copolymer. *Macromolecules* 2012;45:9531–8.
- [90] Wołoszczuk S, Banaszak M, Knychala P, Radosz M. Monte Carlo phase diagram of symmetric diblock copolymer in selective solvent. *Macromolecules* 2008;41:5945–51.
- [91] Knychala P, Banaszak M, Polanowski P. Phase behavior of block copolymer solutions in thin films studied by Monte Carlo simulations. *Soft Matter* 2012;8:6638–45.
- [92] Gotrik KW, Hannon AF, Son JG, Keller B, Alexander-Katz A, Ross CA. Morphology control in block copolymer films using mixed solvent vapors. *ACS Nano* 2012;6:8052–9.
- [93] Zhou L, Liu Y, Sun B. Solvents-induced structure transitions in copolymer films. *Adv Mater Res* 2013;684:94–8.
- [94] Rudov AA, Patyukova ES, Neratova IV, Khalatur PG, Posselt D, Papadakis CM, et al. Structural changes in lamellar diblock copolymer thin films upon swelling in non-selective solvents. *Macromolecules* 2013;46:5786–95.
- [95] Hur SM, Khaira GS, Ramírez-Hernández A, Müller M, Nealey PF, de Pablo JJ. Simulation of defect reduction in block copolymer thin films by solvent annealing. *ACS Macro Lett* 2015;4: 11–5.
- [96] Tsige M, Mattsson TR, Grest GS. Morphology of evaporated multi-block copolymer membranes studied by molecular dynamics simulations. *Macromolecules* 2004;37:9132–8.
- [97] Buxton GA, Clarke N. Ordering polymer blend morphologies via solvent evaporation. *Europhys Lett* 2007;78, 56006/1–5.
- [98] Morita H, Ozawa T, Kobayashi N, Fukunaga H, Doi M. Dissipative particle dynamics study for the phase separated structures of polymer thin film caused by solvent evaporation. *Nihon Reoroji Gakkaishi* 2008;36:93–8.
- [99] Phillip WA, Hillmyer MA, Cussler EL. Cylinder orientation mechanism in block copolymer thin films upon solvent evaporation. *Macromolecules* 2010;43:7763–70.
- [100] Neratova IV, Pavlov AS, Khalatur PG. Effect of a solvent on self-organization in nanofilms: modeling by the dissipative particle dynamics method. *Polymer Sci Ser A* 2010;52:959–69.
- [101] Li YC, Liu H, Huang XR, Sun CC. Evaporation- and surface-induced morphology of symmetric diblock copolymer thin films: a multibody dissipative particle dynamics study. *Mol Simul* 2011;37:875–83.
- [102] Stenbeck-Fermor A, Rudov AA, Gumerov RA, Tsarkova LA, Böker A, Möller M, et al. Morphology-controlled kinetics of solvent uptake by block copolymer films in nonselective solvent vapors. *ACS Macro Lett* 2014;3:803–7.
- [103] Paradiso SP, Delaney KT, García-Cervera CJ, Ceniceros HD, Fredrickson GH. Block copolymer self assembly during rapid solvent evaporation: insights into cylinder growth and stability. *ACS Macro Lett* 2014;3:16–20.
- [104] Berezhkin AV, Papadakis CM, Potemkin II. Vertical domain orientation in cylinder-forming diblock copolymer films upon solvent vapor annealing. *Macromolecules* 2016;49:415–24.
- [105] Polovnikov KE, Gumerov RA, Potemkin II. Stress-induced solvent redistribution in lamellae-forming diblock copolymer systems. *Macromolecules* 2016;49:6599–608.
- [106] Lo TY, Ho RM, Georgopoulos P, Avgoropoulos A, Hashimoto T. Direct visualization of order-order transitions in silicon-containing block copolymers by electron tomography. *ACS Macro Lett* 2013;2:190–4.
- [107] Helfand E, Tagami Y. Theory of the interface between immiscible polymers. II. *J Chem Phys* 1972;56:3592–601.
- [108] Whitmore MD, Noolandi J. Self-consistent theory of block copolymer blends: neutral solvent. *J Chem Phys* 1990;93:2946–55.
- [109] Banaszak M, Whitmore MD. Self-consistent theory of block copolymer blends: selective solvent. *Macromolecules* 1992;25:3406–12.
- [110] Vavasour JD, Whitmore MD. Effects of solubilized homopolymer on lamellar diblock copolymer structures. *Macromolecules* 2001;34:3471–83.
- [111] Di Z, Posselt D, Smilgies DM, Li R, Rauscher M, Potemkin II, et al. Stepwise swelling of a thin film of lamellae-forming poly(styrene-*b*-butadiene) in cyclohexane vapor. *Macromolecules* 2012;45:5185–95.
- [112] Shibayama M, Hashimoto T, Kawai H. Ordered structure in block polymer solutions. 1. Selective solvents. *Macromolecules* 1983;16:16–28.
- [113] Shibayama M, Hashimoto T, Hasegawa H, Kawai H. Ordered structure in block polymer solutions. 3. Concentration dependence of microdomains in nonselective solvents. *Macromolecules* 1983;16:1427–33.
- [114] Hashimoto T, Tanaka T, Hasegawa H. Ordered structure in mixtures of a block copolymer and homopolymers. 2. Effects of molecular weights of homopolymers. *Macromolecules* 1990;23:4378–86.
- [115] Hanley KJ, Lodge TP. Effect of dilution on a block copolymer in the complex phase window. *J Polym Sci Part B: Polym Phys* 1998;36:3101–13.
- [116] Hanley KJ, Lodge TP, Huang CI. Phase behavior of a block copolymer in solvents of varying selectivity. *Macromolecules* 2000;33:5918–31.
- [117] Lai CJ, Russel WB, Register RA. Scaling of domain spacing in concentrated solutions of block copolymers in selective solvents. *Macromolecules* 2002;35:4044–9.
- [118] Lodge TP, Hanley KJ, Pudil B, Alahapperuma V. Phase behavior of block copolymers in a neutral solvent. *Macromolecules* 2003;36:816–22.
- [119] Naughton JR, Matsen MW. Limitations of the dilution approximation for concentrated block copolymer/solvent mixtures. *Macromolecules* 2002;35:5688–96.
- [120] Di Z, Posselt D, Smilgies DM, Papadakis CM. Structural rearrangements in a lamellar diblock copolymer thin film during treatment with saturated solvent vapor. *Macromolecules* 2010;43: 418–27.
- [121] Zhang J, Posselt D, Smilgies DM, Perlich J, Kyriakos K, Jaksch S, et al. Lamellar diblock copolymer thin films during solvent vapor annealing studied by GISAXS: different behavior of parallel and perpendicular lamellae. *Macromolecules* 2014;47:5711–8.
- [122] Schubert DW, Dunkel T. Spin coating from a molecular point of view: its concentration regimes, influence of molar mass and distribution. *Mater Res Innov* 2003;8:314–21.
- [123] Perlich J, Körstgens V, Metwalli E, Schulz L, Georgii R, Müller-Buschbaum P. Solvent content in thin spin-coated polystyrene homopolymer films. *Macromolecules* 2009;42:337–44.
- [124] Reinhardt KA, Kern W, editors. *Handbook of semiconductor wafer cleaning technology*. Noyes, NJ: Park Ridge; 2008. p. 722.
- [125] Müller-Buschbaum P. Influence of surface cleaning on dewetting of thin polystyrene films. *Eur Phys J E* 2003;12:443–8.
- [126] Sherman R. Carbon dioxide snow cleaning. *Part Sci Technol* 2007;25:37–57.
- [127] Wang W, Metwalli E, Perlich J, Papadakis CM, Cubitt R, Müller-Buschbaum P. Cyclic switching of water storage in thin block copolymer films containing poly(N-isopropylacrylamide). *Macromolecules* 2009;42:9041–51.
- [128] Kim SH, Misner MJ, Xu T, Kimura M, Russell TP. Highly oriented and ordered arrays from block copolymers via solvent evaporation. *Adv Mater* 2004;16:226–31.
- [129] Cavicchi KA, Berthiaume KJ, Russell TP. Solvent annealing thin films of poly(isoprene-*b*-lactide). *Polymer* 2005;46:11635–9.
- [130] Rider DA, Cavicchi KA, Vanderark L, Russell TP, Manners I. Orientationally controlled nanoporous cylindrical domains in polystyrene-*b*-poly(ferrocenylethylmethylsilane) block copolymer films. *Macromolecules* 2007;40:3790–6.

- [131] Papadakis CM, Di Z, Posselt D, Smilgies DM. Structural instabilities in lamellar diblock copolymer thin films during solvent vapor uptake. *Langmuir* 2008;24:13815–8.
- [132] Bosworth JK, Black CT, Ober CK. Selective area control of self-assembled pattern architecture using a lithographically patternable block copolymer. *ACS Nano* 2009;3:1761–6.
- [133] Jeong JW, Park WI, Kim MJ, Ross CA, Jung YS. Highly tunable self-assembled nanostructures from a poly(2-vinylpyridine-*b*-dimethylsiloxane) block copolymer. *Nano Lett* 2011;11:4095–101.
- [134] Sepe A, Černoch P, Štěpánek P, Hoppe ET, Papadakis CM. Creation of lateral structures in diblock copolymer thin films during vapor uptake and subsequent drying – effect of film thickness. *Eur Polym J* 2014;50:87–96.
- [135] Dourdain S, Rezaire A, Mehdi A, Ocko BM, Gibaud A. Real time GISAXS study of micelle hydration in CTAB templated silica thin films. *Physica B* 2005;357:180–4.
- [136] Zettl U, Knoll A, Tsarkova L. Effect of confinement on the mesoscale and macroscopic swelling of thin block copolymer films. *Langmuir* 2009;26:6610–7.
- [137] Albert JNL, Young WS, Lewis III RL, Bogart TD, Smith JR, Epps III TH. Systematic study of the effect of solvent removal rate on the morphology of solvent vapor annealed ABA triblock copolymer thin films. *ACS Nano* 2012;6:459–66.
- [138] Gu X, Gunkel I, Hexemer A, Gu W, Russell TP. An in situ grazing incidence X-ray scattering study of block copolymer thin films during solvent vapor annealing. *Adv Mater* 2013;26:273–81.
- [139] Zhang J, Posselt D, Sepe A, Shen X, Perlich J, Smilgies DM, et al. Structural evolution of perpendicular lamellae in diblock copolymer thin films during solvent vapor treatment investigated by grazing-incidence small-angle X-ray scattering. *Macromol Rapid Commun* 2013;34:1289–95.
- [140] Gu X, Gunkel I, Hexemer A, Russell TP. Solvent vapor annealing of block copolymer thin films: removal of processing history. *Colloid Polym Sci* 2014;292:1795–802.
- [141] Zhang J, Posselt D, Sepe A, Shen X, Perlich J, Smilgies DM, et al. Complex macrophase separated nanostructure induced by microphase separation in binary blends of lamellar diblock copolymer thin films. *Macromol Rapid Commun* 2014;35:1622–9.
- [142] Zhang J, Luo Z, Martens B, Quan Z, Kumbhar A, Porter N, et al. Reversible Kirkwood–Alder transition observed in Pt3Cu2 nanocatahedron assemblies under controlled solvent annealing/drying conditions. *J Am Chem Soc* 2012;134:14043–9.
- [143] Smilgies DM, Busch P, Papadakis CM, Posselt D. Characterization of polymer thin films with small-angle X-ray scattering under grazing incidence (GISAXS). *Synchrotron Rad News* 2002;15(5):35–42.
- [144] Paik MY, Bosworth JK, Smilgies DM, Schwartz EL, André X, Ober CK. Reversible morphology control in block copolymer films via solvent vapor processing: an in situ GISAXS study. *Macromolecules* 2010;43:4253–60.
- [145] Park S, Kim B, Xu J, Hofmann T, Ocko BM, Russell TP. Lateral ordering of cylindrical microdomains under solvent vapor. *Macromolecules* 2009;42:1278–84.
- [146] Kim JM, Kim A, Park WI, Hur YH, Jeong JW, Sim DM, et al. Eliminating the trade-off between the throughput and pattern quality of sub-15 nm directed self-assembly via warm solvent annealing. *Adv Funct Mater* 2015;25:306–15.
- [147] Kazimirov A, Smilgies DM, Shen Q, Xiao X, Hao Q, Fontes E, et al. Multilayer X-ray optics at CHESS. *J Synchrotron Rad* 2006;13:204–10.
- [148] Smilgies DM. Scherrer grain-size analysis adapted to grazing-incidence scattering with area detectors. *J Appl Crystallogr* 2009;42:1030–4.
- [149] Sinha SK, Sirota EB, Garoff S, Stanley HB. X-ray and neutron scattering from rough surfaces. *Phys Rev B* 1988;38:2297–311.
- [150] Müller-Buschbaum P, Bauer E, Maurer E, Roth SV, Gehrke R, Burghammer M, et al. Large scale and local scale structures in polymer blend films: a GISAXS and sub-microbeam GISAXS investigation. *J Appl Crystallogr* 2007;40:s341–5.
- [151] Gruner SM, Tate MW, Eikenberry EF. Charge-coupled device area X-ray detectors. *Rev Sci Instrum* 2002;73:2815–42.
- [152] Smilgies DM, Li R, Giri G, Chou KW, Diao Y, Bao Z, et al. Look fast: crystallization of conjugated molecules during solution shearing probed in-situ and in real time by X-ray scattering. *Phys Status Solidi Rapid Res Lett* 2013;7:177–9.
- [153] Jiang Z, Lee DR, Narayanan S, Wang J, Sinha SK. Waveguide-enhanced grazing-incidence small-angle X-ray scattering of buried nanostructures in thin films. *Phys Rev B* 2011;84, 075440/1–13.
- [154] Lee B, Park I, Yoon J, Park S, Kim J, Kim KW, et al. Structural analysis of block copolymer thin films with grazing incidence small-angle X-ray scattering. *Macromolecules* 2005;38:4311–23.
- [155] Busch P, Rauscher M, Smilgies DM, Posselt D, Papadakis CM. Grazing-incidence small-angle X-ray scattering from thin polymer films with lamellar structures – the scattering cross section in the distorted-wave Born approximation. *J Appl Crystallogr* 2006;39:433–42.
- [156] Als-Nielsen J, McMorrow D. Elements of modern X-ray physics. 2nd ed. New York: John Wiley & Sons; 2001. p. 432.
- [157] Lazzari R. IsGISAXS: a program for grazing-incidence small-angle X-ray scattering analysis of supported islands. *J Appl Crystallogr* 2002;35:406–21.
- [158] Babonneau D. FitGISAXS: software package for modelling and analysis of GISAXS data using IGOR Pro. *J Appl Crystallogr* 2010;43:929–36.
- [159] Busch P, Posselt D, Smilgies DM, Rauscher M, Papadakis CM. Inner structure of thin films of lamellar poly(styrene-*b*-butadiene) diblock copolymers as revealed by grazing-incidence small-angle scattering. *Macromolecules* 2007;40:630–40.
- [160] Smilgies DM, Heitsch AT, Korgel BA. Stacking of hexagonal nanocrystal layers during Langmuir–Blodgett deposition. *J Phys Chem B* 2012;116:6017–26.
- [161] Heitsch AT, Patel RN, Goodfellow BW, Smilgies DM, Korgel BA. GISAXS characterization of order in hexagonal monolayers of FePt nanocrystals. *J Phys Chem C* 2010;114:14427–32.
- [162] Busch P, Posselt D, Smilgies DM, Rheinländer B, Kremer F, Papadakis CM. Lamellar diblock copolymer thin films investigated by tapping mode atomic force microscopy: molar-mass dependence of surface ordering. *Macromolecules* 2003;36:8717–27.
- [163] Busch P, Rauscher M, Moulin JF, Müller-Buschbaum P. Debye–Scherrer rings from block copolymer films with powder-like order. *J Appl Crystallogr* 2011;44:370–9.
- [164] Park I, Lee B, Ryu J, Im K, Yoon J, Ree M, et al. Epitaxial phase transition of polystyrene-*b*-polyisoprene from hexagonally perforated layer to gyroid phase in thin film. *Macromolecules* 2005;38:10532–6.
- [165] Shin C, Ryu DY, Huh J, Kim JH, Kim KW. Order-to-order transitions of block copolymer in film geometry. *Macromolecules* 2009;42:2157–60.
- [166] Papadakis CM, Darko C, Di Z, Troll K, Metwalli E, Timmann A, et al. Surface-induced breakout crystallization in cylinder-forming P(*i*-*b*-EO) diblock copolymer thin films. *Eur Phys J E* 2011;34:7–14.
- [167] Cavicchi KA, Russell TP. Solvent annealed thin films of asymmetric polyisoprene–polylactide diblock copolymers. *Macromolecules* 2007;40:1181–6.
- [168] Jin S, Hirai T, Ahn B, Rho Y, Kim KW, Kakimoto MA, et al. Synchrotron grazing incidence X-ray scattering study of the morphological structures in thin films of a polymethacrylate diblock copolymer bearing POSS moieties. *J Phys Chem B* 2010;114:8033–42.
- [169] Stein GE, Kramer Ej, Li X, Wang J. Layering transitions in thin films of spherical-domain block copolymers. *Macromolecules* 2007;40:2453–60.
- [170] Xu T, Goldbach JT, Misner MJ, Kim S, Gibaud A, Gang O, et al. Scattering study on the selective solvent swelling induced surface reconstruction. *Macromolecules* 2004;37:2972–7.
- [171] Papadakis CM, Busch P, Posselt D, Smilgies DM. Morphological transition in thin lamellar diblock copolymer films as revealed by combined GISAXS and AFM studies. *Adv Solid State Phys* 2004;44:327–38.
- [172] Tang C, Tracz A, Kruk M, Zhang R, Smilgies DM, Matyjaszewski K, et al. Long-range ordered thin films of block copolymers by zone-casting and their thermal conversion into ordered nanostructured carbon. *J Am Chem Soc* 2005;127:6918–9.
- [173] Yoon J, Yang SY, Lee B, Joo W, Heo K, Kimb JK, et al. Nondestructive quantitative synchrotron grazing incidence X-ray scattering analysis of cylindrical nanostructures in supported thin films. *J Appl Crystallogr* 2007;40:305–12.
- [174] Metwalli E, Perlich J, Wang W, Diethert A, Roth SV, Papadakis CM, et al. Morphology of semicrystalline diblock copolymer thin films upon directional solvent vapor flow. *Macromol Chem Phys* 2010;21:2102–8.
- [175] Metwalli E, Nie M, Körstgens V, Perlich H, Roth SV, Müller-Buschbaum P. Morphology of lithium-containing diblock copolymer thin films. *Macromol Chem Phys* 2011;212:1742–50.
- [176] Anonymous Small-angle scattering facilities; 2013. <http://www.nanonanonano.net/tmp/smallangl/facilities-list.html> [accessed September 2016].

- [177] Smilgies DM GISAXS and GIWAXS; 2014. <http://www.classe.cornell.edu/~dms79/gisaxs/GISAXS.html> [accessed September 2016].
- [178] Meyer A GISAXS. <http://www.gisaxs.de> 2015 [accessed September 2016].
- [179] Lazzari R IsGISAXS: a tool for grazing incidence small angle X-ray scattering analysis for nanostructures; 2015. <http://www.insp.jussieu.fr/oxydes/IsGISAXS/figures/doc/manual.html> [accessed September 2016].
- [180] Anonymous GISAXS comm.unity website; 2014. www.gisaxs.com [accessed September 2016].
- [181] Hammersley A The Fit2D home page; 2016. <http://www.esrf.eu/computing/scientific/FIT2D> [accessed September 2016].
- [182] Benecke G, Wagermaier W, Li C, Schwartzkopf M, Flucke G, Hoerth R, et al. A customizable software for fast reduction and analysis of large X-ray scattering data sets: applications of the new DPDAK package to small-angle X-ray scattering and grazing-incidence small-angle X-ray scattering. *J Appl Crystallogr* 2014;47:1797–803.
- [183] Lyon O Gisaxs.org; 2016. <http://www.gisaxs.org> [accessed September 2016].
- [184] Hillhouse HW NANOCELL; 2016. <http://faculty.washington.edu/h2/simulation.html> [accessed September 2016].
- [185] Tate MP, Urade VN, Kowalski JD, Wei TC, Hamilton BD, Eggiman BW, et al. Simulation and interpretation of 2D diffraction patterns from self-assembled nanostructured films at arbitrary angles of incidence: from grazing incidence (above the critical angle) to transmission perpendicular to the substrate. *J Phys Chem B* 2006;110:9882–92.
- [186] Durniak C, Ganeva M, Pospelov G, Van Herck W, Wuttke J. BornAgain – software for simulating and fitting X-ray and neutron small-angle scattering at grazing incidence; 2015. <http://www.bornagainproject.org> [accessed September 2016].
- [187] Chourou ST, Sarje A, Li XS, Chan ER, Hexemer A. HipGISAXS: a high-performance computing code for simulating grazing-incidence X-ray scattering data. *J Appl Crystallogr* 2013;46:1781–95.
- [188] Albalak RJ, Capel MS, Thomas EL. Solvent swelling of roll-cast triblock copolymer films. *Polymer* 1998;39:1647–56.
- [189] Kim G, Libera M. Morphological development in solvent-cast polystyrene-polybutadiene-polystyrene (SBS) triblock copolymer thin films. *Macromolecules* 1998;31:2569–77.
- [190] Fukunaga K, Elbs H, Magerle R, Krausch G. Large-scale alignment of ABC block copolymer microdomains via solvent vapor treatment. *Macromolecules* 2000;33:947–53.
- [191] Fukunaga K, Hashimoto T, Elbs H, Krausch G. Self-assembly of a lamellar ABC triblock copolymer thin film. *Macromolecules* 2002;35:4406–13.
- [192] Kim SH, Misner MJ, Yang L, Gang O, Ocko BM, Russell TP. Salt complexation in block copolymer thin films. *Macromolecules* 2006;39:8473–9.
- [193] Gowd EB, Böhme M, Stamm M. In situ GISAXS study on solvent vapour induced orientation switching in PS-*b*-P4VP block copolymer thin films. IOP Conf Ser Mater Sci Eng 2010;14, 012015/1–6.
- [194] Gowd EB, Koga T, Endoh MK, Kumar K, Stamm M. Pathways of cylindrical orientations in PS-*b*-P4VP diblock copolymer thin films upon solvent vapor annealing. *Soft Matter* 2014;10:7753–61.
- [195] Bai W, Yager KG, Ross CA. In situ characterization of the self-assembly of a polystyrene-polydimethylsiloxane block copolymer during solvent vapor annealing. *Macromolecules* 2015;48:8574–84.
- [196] Smilgies DM, Li R, Di Z, Darko C, Papadakis CM, Posselt D. Probing the self-organization kinetics in block copolymer films. Mater Res Soc Symp Proc 2009;1147:0001.
- [197] Gunkel I, Gu X, Sun Z, Schable E, Hexemer A, Russell TP. An *in-situ* GISAXS study of selective solvent vapor annealing in thin block copolymer films: symmetry breaking of in-plane sphere order upon deswelling. *J Polym Sci Part B: Polym Phys* 2016;54:331–8.
- [198] Gu X, Gunkel I, Hexemer A, Russell TP. Controlling domain spacing and grain size in cylindrical block copolymer thin films by means of thermal and solvent vapor annealing. *Macromolecules* 2016;49:3373–81.
- [199] Sepe A, Zhang J, Perlich J, Smilgies DM, Posselt D, Papadakis CM. Towards an equilibrium structure in lamellar diblock copolymer thin films using solvent vapor annealing – an *in-situ* time-resolved GISAXS study. *Eur Polym J* 2016;81:607–20.
- [200] Doshi DA, Gibaud A, Goletto V, Lu MC, Gerung H, Ocko B, et al. Peering into the self-assembly of surfactant templated thin-film silica mesophases. *J Am Chem Soc* 2003;125:11646–55.
- [201] Roth SV, Herzog G, Körstgens V, Buffet A, Schwartzkopf M, Perlich J, et al. *In situ* observation of cluster formation during nanoparticle solution casting on a colloidal film. *J Phys: Condens Matter* 2011;23, 254208/1–9.
- [202] Gibaud A, Gross D, Smarsly B, Baptiste A, Bardeau JF, Babonneau F, et al. Evaporation-controlled self-assembly of silica surfactant mesophases. *J Phys Chem B* 2003;107:6114–8.
- [203] Metwalli E, Körstgens V, Schrage K, Meier R, Kaune G, Buffet A, et al. Cobalt nanoparticles growth on a block copolymer thin film: a time-resolved GISAXS study. *Langmuir* 2013;29:6331–40.
- [204] Ramesh N, Davis PK, Zielinski JM, Danner RP, Duda JL. Application of free-volume theory to self diffusion of solvents in polymers below the glass transition temperature: a review. *J Polym Sci Part B: Polym Phys* 2011;49:1629–44.
- [205] Wodo O, Ganapathysubramanian B. How do evaporating thin films evolve? Unravelling phase-separation mechanisms during solvent-based fabrication of polymer blends. *Appl Phys Lett* 2014;105, 153104/1–4.
- [206] Wang C, Lee DH, Hexemer A, Kim MI, Zhao W, Hasegawa H, et al. Defining the nanostructured morphology of triblock copolymers using resonant soft X-ray scattering. *Nano Lett* 2011;11:3906–11.
- [207] Müller-Buschbaum P, Gutmann JS, Cubitt R, Petry W. Grazing incidence small-angle neutron scattering – an advanced scattering technique for the investigation of nanostructured polymer films. *Physica B* 2004;350:207–10.
- [208] Müller-Buschbaum P. Grazing incidence small angle neutron scattering: challenges and possibilities. *Polym J* 2013;45:34–42.
- [209] Metwalli E, Moulin JF, Rauscher M, Kaune G, Ruderer MA, Van Bürk U, et al. Structural investigation of thin diblock copolymer films using time-of-flight grazing-incidence small-angle neutron scattering. *J Appl Crystallogr* 2011;44:84–92.
- [210] Müller-Buschbaum P, Kaune G, Haese-Seiller M, Moulin JF. Morphology determination of defect-rich diblock copolymer films with time-of-flight grazing incidence small angle neutron scattering. *J Appl Crystallogr* 2014;47:1228–37.
- [211] Hayat J, Mitra I, Qiao Y, Stein GE, Tang C. Improving humidity-controlled solvent annealing processes for block copolymer poly(ethylene oxide)-*b*-polystyrene. *Eur Polym J* 2015;71:476–89.
- [212] Seguin G, Zanenga F, Giannaria TJ, Ceresoli M, Sparnacci K, Antonioli D, et al. Enhanced lateral ordering in cylinder forming PS-*b*-PMMA block copolymers exploiting the entrapped solvent. *ACS Appl Mater Interfaces* 2016;8:8280–8.
- [213] Jung YS, Ross CA. Solvent vapor induced tunability of self-assembled block copolymer patterns. *Adv Mater* 2009;21:2540–5.
- [214] Albert JNL, Bogart TD, Lewis RL, Beers KL, Fasolka MJ, Hutchinson JB, et al. Gradient solvent vapor annealing of block copolymer thin films using a microfluidic mixing device. *Nano Lett* 2011;11:1351–7.
- [215] Kim B, Hong SW, Park S, Xu J, Hong SK, Russell TP. Phase transition behavior in thin films of block copolymers by use of immiscible solvent vapors. *Soft Matter* 2011;7:443–7.
- [216] Seppala JE, Lewis RL, Epps TH. Spatial and orientation control of cylindrical nanostructures in ABA triblock copolymer thin films by raster solvent annealing (RSVA). *ACS Nano* 2012;6:9855–62.
- [217] Park WI, Tong S, Liu Y, Jung IW, Roelofs A, Hong S. Tunable and rapid self-assembly of block copolymers using mixed solvent vapors. *Nanoscale* 2014;6:15216–21.
- [218] Chavis MA, Smilgies DM, Wiesner UB, Ober CK. Widely tunable morphologies in block copolymer thin films through solvent vapor annealing using mixtures of selective solvents. *Adv Funct Mater* 2015;25:3057–65.
- [219] Park WI, Choi YJ, Yun JM, Hong SW, Jung YS, Kim KH. Enhancing the directed self-assembly kinetics of block copolymers using binary solvent mixtures. *ACS Appl Mater Interfaces* 2015;7:25843–50.
- [220] Cetintas M, Kamperman M. Self-assembly of PS-*b*-PNIPAM-*b*-PS block copolymer thin films via selective solvent annealing. *Polymer* 2016, <http://dx.doi.org/10.1016/j.polymer.2016.08.033>.
- [221] Roth SV, Burghammer M, Riekel C, Müller-Buschbaum P, Diethert A, Panagiotou P, et al. Self-assembled gradient nanoparticle-polymer multilayers investigated by an advanced characterisation method: microbeam grazing incidence X-ray scattering. *Appl Phys Lett* 2003;82:1935–7.
- [222] Li R, Cornaby S, Kamperman M, Smilgies DM. Nanocomposite characterization on multiple length scales using μ SAXS. *J Synchrotron Rad* 2011;18:697–701.
- [223] Park S, Lee DH, Xu J, Kim B, Hong SW, Jeong U, et al. Macroscopic 10-terabit-per-square-inch arrays from block copolymers with lateral order. *Science* 2009;323:1030–3.
- [224] Luo M, Epps III TH. Directed block copolymer thin film self-assembly: emerging trends in nanopattern fabrication. *Macromolecules* 2013;46:7567–79.

- [225] Kim E, Ahn H, Park S, Lee H, Lee M, Lee S, et al. Directed assembly of high molecular weight block copolymers: highly ordered line patterns of perpendicularly oriented lamellae with large periods. *ACS Nano* 2013;7:1952–60.
- [226] Dinachali SS, Bai W, Tu KH, Choi HK, Zhang J, Kreider ME, et al. Thermo-solvent annealing of polystyrene-polydimethylsiloxane block copolymer thin films. *ACS Macro Lett* 2015;4:500–4.
- [227] Sunday DF, Kline RJ. Reducing block copolymer interfacial widths through polymer additives. *Macromolecules* 2015;48:679–86.
- [228] Schaffer CJ, Wang C, Hexemer A, Müller-Buschbaum P. Grazing incidence resonant soft X-ray scattering for analysis of multi-component polymer-fullerene blend thin films. *Polymer* 2016, <http://dx.doi.org/10.1016/j.polymer.2016.05.056>.